ResearchGate

See discussions, stats, and author profiles for this publication at: https://www.researchgate.net/publication/316462778

Extracting the intertidal extent and topography of the Australian coastline from a 28 year time series of Landsat observations

Article *in* Remote Sensing of Environment · June 2017

DOI: 10.1016/j.rse.2017.04.009

CITATIONS
0

READS
129

4 authors, including:

Stephen Sagar
Geoscience Australia
15 PUBLICATIONS **60** CITATIONS

SEE PROFILE

Leo Lymburner
Geoscience Australia
47 PUBLICATIONS **1,027** CITATIONS

SEE PROFILE

Some of the authors of this publication are also working on these related projects:

Project

Australian Geoscience Data Cube View project

All content following this page was uploaded by Stephen Sagar on 03 May 2017.

The user has requested enhancement of the downloaded file. All in-text references underlined in blue are added to the original document and are linked to publications on ResearchGate, letting you access and read them immediately.

Remote Sensing of Environment 195 (2017) 153–169

Contents lists available at ScienceDirect

Remote Sensing of Environment

journal homepage: www.elsevier.com/locate/rse

Extracting the intertidal extent and topography of the Australian coastline from a 28 year time series of Landsat observations

Stephen Sagar [a,*], Dale Roberts [a,b], Biswajit Bala [a], Leo Lymburner [a]

[a] National Earth and Marine Observations Branch, Geoscience Australia, Canberra, Australia
[b] Australian National University, Canberra, Australia

ARTICLE INFO

Article history:
Received 10 December 2016
Received in revised form 8 March 2017
Accepted 11 April 2017
Available online xxxx

Keywords:
Landsat
Time-series
Tidal modelling
Intertidal
Coastal
Elevation
Topography
Image compositing

ABSTRACT

The physical environment of the intertidal zone presents a number of challenges which make traditional surveying methods difficult to implement; whilst the acquisition cost of airborne elevation data can be prohibitive beyond localised applications. Remote sensing data from earth observation satellites has been well established as a method for mapping the extent and elevation profile of the intertidal zone; however the majority of these applications are local in nature, and based on analysis of a limited number of individual image observations.

In this paper we outline an automated methodology to model the intertidal extent and topography of the Australian coastline, that leverages a full time series of Landsat observations from 1987 to 2015 managed in the Australian Geoscience Data Cube (AGDC). Our approach reframes the analysis from time of acquisition into the tidal domain through the use of a continental scale tidal model, combined with a median pixel compositing of Normalised Difference Water Index (NDWI) stacks, to robustly estimate the tidal extent and elevation profile across the observed tidal range. We demonstrate the ability of a median-based compositing approach to deal effectively with data quality, modelling outliers and other issues that commonly affect single scene methodologies. Our new framework enables us to produce a continental-scale intertidal model, detailing intertidal zone topography at a 25 m spatial scale.

We then demonstrate the potential of the modelling framework to derive digital elevation data based on tidal model attribution, validating our models against in-situ GPS observations, before discussing issues that must be addressed to move this capability to a continental scale. The ability of the model to examine coastal stability is introduced, in the context of the conceptual reframing of the data into the tidal domain, with a view to furthering this application in future versions of the model.

© 2017 Published by Elsevier Inc.

1. Introduction

1.1. Background

The intertidal zone is an important coastal ecosystem, characterised by high productivity and biodiversity and providing habitat for migratory shorebirds worldwide (Brockmann and Stelzer, 2008; Galbraith et al., 2002). Tidal flats also provide critical coastal protection from extreme storm events, and are often a component of the coastal geomorphologic system around high value commercial asset sites such as ports, harbours and recreational areas (Bell et al., 2016; Healy et al., 2002). Once considered one of the areas of the natural environment relatively unaffected by man (Mason et al., 2010), the intertidal zone is coming under increased pressure from land reclamation, human impacts and sea level rise (Airoldi and Beck, 2007; Chen et al., 2016; Kirwan and Megonigal, 2013; Murray et al., 2014).

Capturing information on the extent and topography of the intertidal zone, particularly at a continental scale, is a challenging and costly exercise. The physical environment of tidal flats makes traditional surveying methods difficult to implement, and acquisition of Light Detection and Ranging (LiDAR) or other airborne elevation data approaches is expensive and subject to the tidal regimes of the study site (Cracknell, 1999; Mason et al., 2010; Ryu et al., 2008). The Australian coastline is over 50,000 km in length, with a minimum estimated intertidal zone of 9,855 km^2, and tidal regimes ranging from micro to macro (Dhanjal-Adams et al., 2016). These intertidal regions vary from remote onshore reefs in the Kimberley region of Western Australia characterised by limited data and logistical access (Kordi et al., 2016); to tidal mudflats extending many kilometres from the shore encompassing important habitats for shorebirds across the Northern Territory and Queensland (Clemens et al., 2016).

Remote sensing has been well established as a technique to locally map and measure the intertidal zone (Bell et al., 2016; Chen and Rau, 1998; Danaher and Collet, 2006; Mason et al., 1995; Murray et al., 2012; Ryu et al., 2002; Zhao et al., 2008). The majority of applications

* Corresponding author at: GPO Box 378, Canberra 2601, Australia.
E-mail address: stephen.sagar@ga.gov.au (S. Sagar).

http://dx.doi.org/10.1016/j.rse.2017.04.009
0034-4257/© 2017 Published by Elsevier Inc.

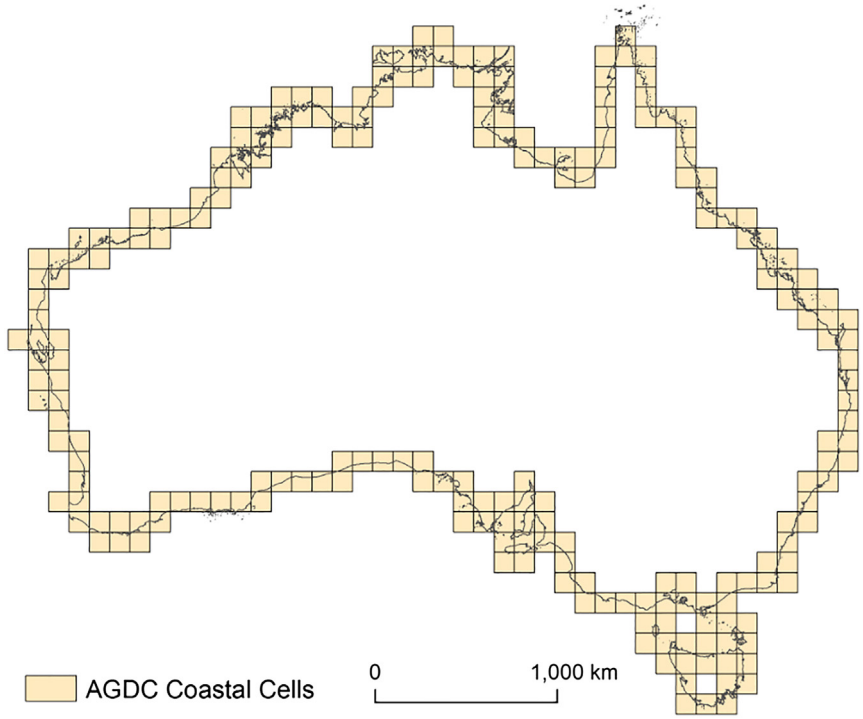

Fig. 1. AGDC Coastal Cells – footprints of each of the 1° by 1° cells used in the modelling process.

involve delineation of the waterline, the boundary between the water body and exposed land surface at the time of image acquisition. This problem has been tackled with a range of data acquisition approaches and analysis methods, ranging from density slicing (Ryu et al., 2008, 2002) or manual digitisation (Zhao et al., 2008) of optical imagery bands, through to edge detection of SAR imagery (Mason et al., 1999). Common to all of these methods is the need to attribute a known tide height or elevation to the data sets used, most often to attribute multiple waterlines for construction of a Digital Elevation Model (DEM).

Attribution of elevation values to tidal waterlines can be completed by utilising tide gauge records (Danaher and Collet, 2006; Zhao et al., 2008), although for long temporal ranges it is often the case that the tidal record may be incomplete or at a coarse temporal resolution, requiring interpolation that can introduce errors (Bell et al., 2016). Hydrodynamic models are often combined with tidal gauge data to improve tidal elevation modelling across complex estuarine environments (Chen and Rau, 1998; Liu et al., 2013; Mason et al., 2010, 1999). These model applications are site-specific and local in nature, with the accuracy of the derived waterline elevations still a function of the model detail and the complexity of the environment (Liu et al., 2013).

Murray et al. (2012) produced the first map of tidal flats of China and the Korean peninsula using 78 Landsat TM and ETM + scenes to map tidal flats over 13,800 km of coastline. Their approach used a water index image differencing procedure, requiring a number of manual pre- and post-processing steps. This approach has recently been applied to the Australian continent (Dhanjal-Adams et al., 2016) to study the distribution of intertidal habitats. Fundamental to this approach is the use of a tidal model to select, for each region, the most suitable low and high tide scene. The inherent limitation of this, and any method which utilises single image scenes, is the requirement that each scene is clear, cloud free, and acquired close to the required tidal height (Chen and Rau, 1998; Ryu et al., 2002). This involves a high degree of manual screening, and can still result in artefacts in the waterline derivation (Dhanjal-Adams et al., 2016). Utilising a sun-synchronous satellite such as Landsat, it is inevitable that the sensor will only observe a sub-portion of the full tidal range at any location, and less frequently at the extremes of low and high tide. This decreases the likelihood of obtaining a clear scene, and can prevent the application of methods in some regions (Dhanjal-Adams et al., 2016).

There have been a limited number of methods that aim to address the restrictions of a single scene approach by leveraging the information provided by a full time-series of observations. Chen et al. (2016) utilise all Landsat observations within 5 year windows to estimate the extent of the Yangstze estuary tidal flats, based on an index-derived water frequency map. Their method does not take tidal information into account, although tide tables were used retrospectively to assess the range of tides observed in each 5 year interval. High tide coastline locations were then visually interpreted from single cloud free images for each time period to produce a tidal flat region. Li and Gong (2016) employ a similar approach and assess the water index annual means of each Landsat pixel to determine the annually inundated area and coastline dynamics of western Florida. Whilst not using tidal information, or aiming to delineate tidal flat from permanent water, they identify the time series mean as effective for addressing distinct variations in horizontal waterline position for coasts and intertidal zones with gentle slopes, even at similar tidal heights. By collecting a time series of observations from a ground based X band marine radar, Bell et al. (2016) correlated radar pixel intensity over time to the corresponding tidal height, enabling an intertidal DEM to be created without the need for waterlines from single images. The authors suggest that their method could be applied to a range of remote sensing data, given a sufficient number of images.

In this paper, we introduce a new approach that draws on some of the ideas mentioned above and leverages the full time series of Landsat observations consisting of more than 200,000 tiles (see Section 2.1) of the coastal area of Australia. Our approach is automated and allows us to map the intertidal extent on a continental scale. It is based on the idea that the analysis of tidal extents can be reframed from time of acquisition of the imagery into the tidal height domain through the use of an ancillary tidal model. We combine this reframed imagery using a pixel compositing approach of derived Normalised Difference Water Index (NDWI) stacks; examining medians to robustly estimate the intertidal extent. This new framework enables us to create a continental-scale intertidal extents model across the full tidal range, detailing

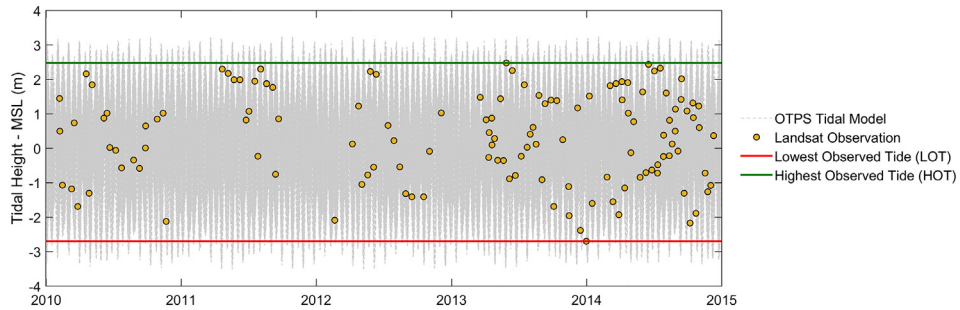

Fig. 2. OTPS Tidal Modelling and Landsat Acquisitions – tidal heights attributed to Landsat acquisitions over a five year period at Darwin, Northern Territory (Cell 130-013), illustrating the concept of highest observed (HOT) and lowest observed (LOT) tides in relation to the full OTPS modelled tidal range.

intertidal zone topography at a 25 m spatial scale. Validation against elevation data collected from Real Time Kinematic (RTK) GPS surveys show close agreement.

1.2. Objectives

Our objective is to develop a consistent, automated and continental scale methodology for characterising the intertidal zone extents and topography of the Australian coast. By utilising the full time series of Landsat data and a tidal modelling process we demonstrate the ability of a median-based compositing approach to deal effectively with data quality, modelling outliers and other issues that commonly affect single scene methodologies.

By assessing the influences of the modelling choices that we have made to enable the automated methodology, we aim to inform developments for future iterations of the product, and demonstrate the potential of transferring time-series ensemble analysis into an alternate (tidal height) domain.

2. Data & models

2.1. The Australian Geoscience Data Cube (AGDC)

The time-series of Landsat data is drawn from 28 years of data from 1987 to 2015 contained within the Australian Landsat data archive (Geoscience Australia, 2015). The archive has been acquired continuously since 1987 by sensors on the Landsat 5, 7 and 8 satellites, at a 25 m pixel resolution and observation frequency of 8–16 days.

Our methodology is based on the particular way in which the Landsat data archive has then been calibrated and restructured (Lewis et al., 2015). The Landsat data was geometrically corrected using the LPGS code developed by the United States Geological Survey (Loveland and Dwyer, 2012), and converted into nadir view angle, bidirectional reflectance distribution function (BRDF), atmospherically corrected surface reflectance (NBAR) using the methods described in Li et al. (2012). Pixel based quality (PQ) metadata (e.g. cloud, cloud shadow, saturation) was calculated for all scenes and stored as bitmasks as described in Sixsmith et al. (2013). These scenes were then spatially segmented into 1° by 1° cells to form a grid of data tiles that cover the full spatial and temporal extent of the archive. This approach, termed the Australian Geoscience Data Cube (AGDC), is pixel-based, rather than the traditional scene-based approach, and incorporates geometric and spectral calibration and quality assurance of each Earth surface reflectance measurement (Lewis et al., 2015). Importantly, each 1° by 1° data tile has a specific date and precise time of acquisition and its geospatial footprint is consistent for all satellite observations of the same area, enabling the direct comparison of observations of a specific location that were acquired days, months or years apart. This also enables variables with a spatial and temporal dependence to be consistently attributed to each tile in an automated workflow.

Of these observations, 221 AGDC cell locations covering the Australian mainland and Tasmanian coastline, consisting of a total of 201,964 tile observations for the 1987–2015 period, have been used in the current study (Fig. 1). The cell numbering convention used in AGDC uses the bottom-left corner location, for instance cell number 122–017 corresponds to a location of 122° longitude and −17° latitude. Each tile was then processed using the PQ bitmasks to exclude pixels flagged as cloud, cloud shadow, or saturated in any of the bands.

2.2. Continental scale tidal modelling

The ability to use tide gauge records to attribute tidal heights to each coastal Landsat tile across the 28 year archive is limited by the variation of temporal and spatial completeness of the tidal record at a continental scale, as is often the case when a continuous time series of water levels is required (Bell et al., 2016). In our work we utilise the Oregon State University Tidal Prediction Software (OTPS), which been used successfully for continental scale time-series tide modelling in both Australia (Dhanjal-Adams et al., 2016) and East Asia (Murray et al., 2012).

We apply the OTPS TPX08 model for our method, consisting of a multi-resolution bathymetric grid solution, with a 1/6° solution in the global open ocean, and a 1/30° local resolution solution to improve modelling in complex shallow water environments (Egbert and Erofeeva, 2010). The OTPS model is based on a system of linear partial differential equations, called Laplace's tidal equations, parametrised with nine harmonic tidal constituents. The model is fitted to track-averaged TOPEX/Poseidon altimeter data collected from 1992 to 2016 and Jason-1 (Poseidon 2) altimeter data from 2002 to 2013, enabling estimation of the tidal height and harmonic constituents at discrete temporal epochs and spatial locations (Egbert and Erofeeva, 2002).

3. Method

The method consisted of four steps: 1) tidal attribution and observation ordering; 2) NDWI index calculation and median composite generation; 4) NDWI thresholding and creation of the relative extents model; 5) deriving an elevation model. In the following subsections we describe each process in more detail.

Table 1
Average number of AGDC Landsat tiles per cell, by intervals of the Observed Tidal Range (OTR).

Tidal interval	0–10%	10–20%	20–30%	30–40%	40–50%	50–60%	60–70%	70–80%	80–90%	90–100%
Mean No. of observations	31	87	115	120	113	106	96	93	71	27

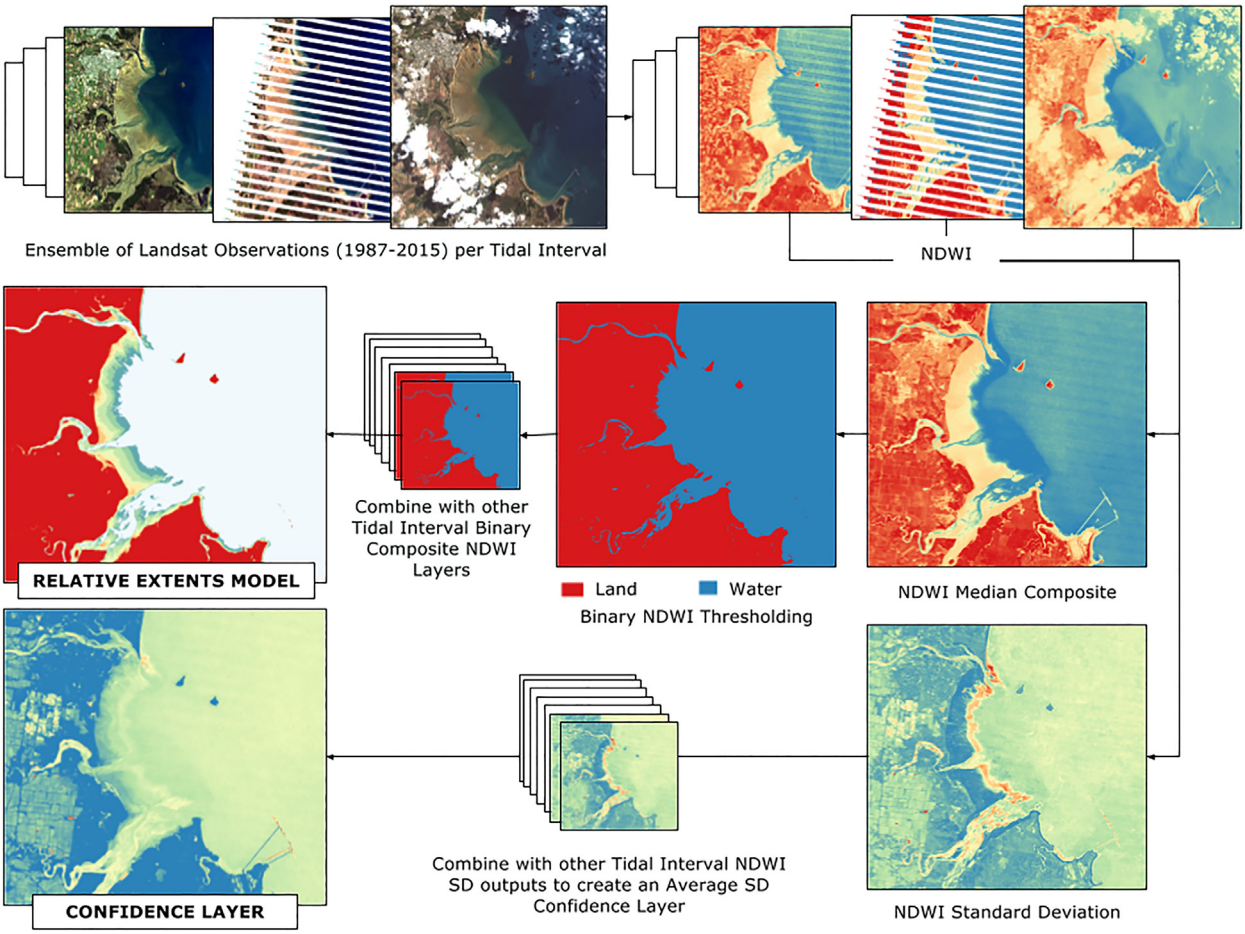

Fig. 3. The Intertidal Extents Model processing sequence – the process shown is completed for each tidal interval ensemble of tile observations. All tiles in the ensemble (regardless of data completeness or quality) are used to generate a median composite NDWI and standard deviation Confidence layer. These interval based outputs are then combined to create the final products.

3.1. Tidal attribution and observation ordering

We attribute each of the Landsat tile observations with a tidal height value from the OTPS TPX08 model. A representative pixel location (the 'tidal post') was determined for each AGDC cell manually. In contrast to the standard rule used by Murray et al. (2012) to position the tidal post, the manual approach was chosen to allow for local variations of coastline complexity and structure to be considered. The tidal post location in each cell is then used to determine the tidal height, relative to Mean Sea Level (MSL), for the full time-series ensemble of tiles at the date and time of acquisition using the OTPS model.

As noted by Bell et al. (2016), who applied a single elevation value to a complex estuary, we also acknowledge that using a single instantaneous tidal elevation value is no doubt a simplification of reality. As part of our stated objectives, we show how we mitigate this by using a median compositing approach to the full time-series (Section 3.2.2), and assess the influence of using a tidal height estimate at a coarse spatial resolution on the modelling process.

The key to our approach is built upon the concept that our tile observations at the coastal cells can be analysed and queried based on considerations other than the natural flow of time, and in particular, the tidal height that we have attributed to a tile (based on the acquisition time of the observation). One can view this approach as switching the ensemble analysis away from the classic temporal domain, as in a traditional time-series analysis, to an alternate (tidal height) domain. This "change of time" approach has been highly effective in pure and applied stochastic process theory and in the development of new financial models (e.g., see Barndorff-Nielsen and Shiryaev, 2010). In our methodology, our change of time consists of sorting the tiles based on the attributed tidal height so that observations are ordered from lowest to highest thus reframing the analysis in terms of tidal height instead of time of imagery acquisition.

Once the tiles are ordered by attributed tidal height, we calculate the observed tidal range (OTR) that consists of the interval between the highest (HOT) and lowest (LOT) observed tidal heights. We then construct a uniform partition of the OTR into 10 intervals. Due to the cyclic nature of the tidal process and Landsat's repeat coverage interval of 16 days, observed tidal heights are not uniformly distributed over the OTR (see Fig. 2 and circular density plots in Fig. 5). As such, our uniform partitioning divides the ensemble of observations into non-uniform sample sizes in each OTR interval.

The number of Landsat acquisitions varies greatly across the Australian continent. Therefore, to ensure a sufficient sample size in each tidal interval for the robust generation of a median composite (Section 3.2.2) for every area across the continent whilst keeping the methodology consistent, it was decided to merge the 80–90% and 90–100% OTR interval ranges for all cells. Whilst we record only a slightly larger number of observations in the lowest 20% of the tidal range in comparison to the highest 20% (Table 1), we made the decision to only merge the highest ranges. This was based on the difference in the spatial extents of the intertidal environment exposed at the upper and lower extremes of the tidal range, as illustrated later in Fig. 7. In this figure we see a

considerable spatial extent at low tide differentiated between the 0–10% and 10–20% intervals. In contrast, the upper intervals of the tidal range show little spatial variation in the modelled exposed surface.

3.2. Index calculation and compositing

3.2.1. Water index selection

For this work we have chosen the Normalised Difference Water Index (NDWI) (McFeeters, 1996) to discriminate between water and non-water pixels. This choice was based on two factors; 1) Simplicity and ease of use with no requirement for training data (i.e., unsupervised classification); 2) Characteristics of the index which have shown it suitable for continental application in the intertidal zone.

The NDWI has been used successfully in continental scale intertidal mapping applications in both Australia (Dhanjal-Adams et al., 2016) and China (Murray et al., 2012), proving to a be a robust index in these environments. The NDWI formula is based on a band ratio between the near infrared (NIR) and visible green band,

$$\mathrm{NDWI} = \frac{Green - NIR}{Green + NIR} \tag{1}$$

where positive NDWI values indicate water, and negative values indicate a non-water or land surface. Whilst simple in application, the use of the NIR band in conjunction with a visible band has been shown to be particularly effective in dealing with the environmental variability characteristic of the intertidal zone. In an ebb tide scenario, Ryu et al. (2002) observed an improved performance of the NIR band over the shortwave infrared band (SWIR) in determining the tidal waterline. Furthermore, when used in conjunction with a visible band Ryu et al. (2002) also showed it to account well for the variability of NIR reflectance associated with turbidity effects on shallow mud flats, as described by Park et al. (2013).

Other water indices such as the Modified Normalized Difference Water Index (MNDWI) (Xu, 2006) and the Automated Water Extraction Index (AWEI) (Feyisa et al., 2014) have been developed to improve water/non-water detection in the presence of built environments and shadows/dark surfaces respectively. Both of these scenarios are of minimal influence in intertidal regions, and a comparative study of the NDWI, MNDWI, and AWEI applied to Landsat data showed NDWI to be most accurate in the non-urban study area (Rokni et al., 2014).

Additional indices have been developed by Danaher and Collet (2006), and more recently Fisher et al. (2016), which have shown an improvement in accuracy when compared to the above mentioned methods. Developed and calibrated using training data from Eastern Australia; an extension of the training database to a continental scale would potentially increase the utility of these indices in future applications of our method.

The main advantage of using a water index based on band ratios is that, combined with our robust estimator (that we detail in the next section) and a choice of threshold to discriminate between water and not-water, it provides a simple unsupervised classification that scales very well to a continental scale as no training data is required.

3.2.2. NDWI median composite generation

For each Landsat tile observation, the NDWI at each pixel was calculated using Eq. (1). In each 1° by 1° cell, this creates an ensemble of NDWI tile images that can be bucketed based on the tidal heights into one of the nine intervals.

Individually, each NDWI image can be viewed as a noisy estimator of water presence (or absence) due to outliers, poorly removed edges of clouds, and other artefacts. We circumvent these problems by performing pixel-based compositing of images within each tidal range bucket. This gives us a pixel-based NDWI composite image for each of the nine tidal intervals (Fig. 3).

A number of image compositing approaches have been proposed in the literature. Approaches such as rule-based compositing (Griffiths et

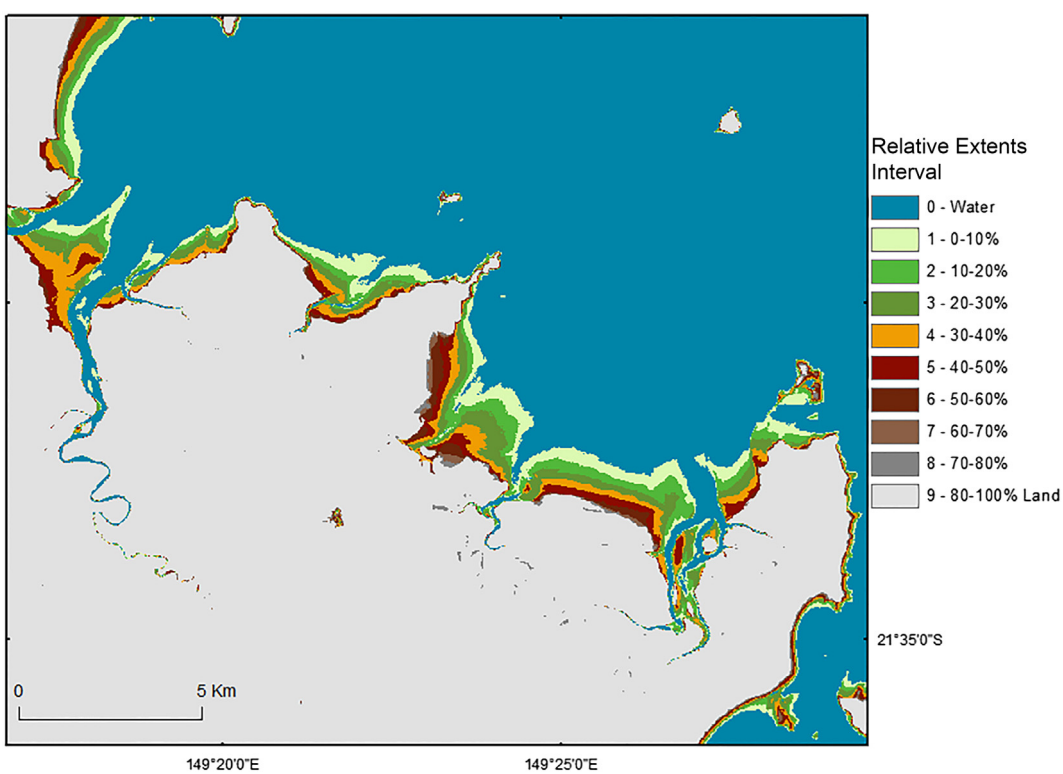

Fig. 4. The Relative Extents Model – example of the relative extents model at Cape Palmerston, QLD (Cell 149-022). Values of 1–8 correspond to areas of intertidal substratum exposed at intervals of the observed tidal range (OTR), creating a topography of the intertidal zone. Values of 9 correspond to areas of land still exposed at the highest 80–100% of the OTR. Values of 0 correspond to areas of water observed across the OTR.

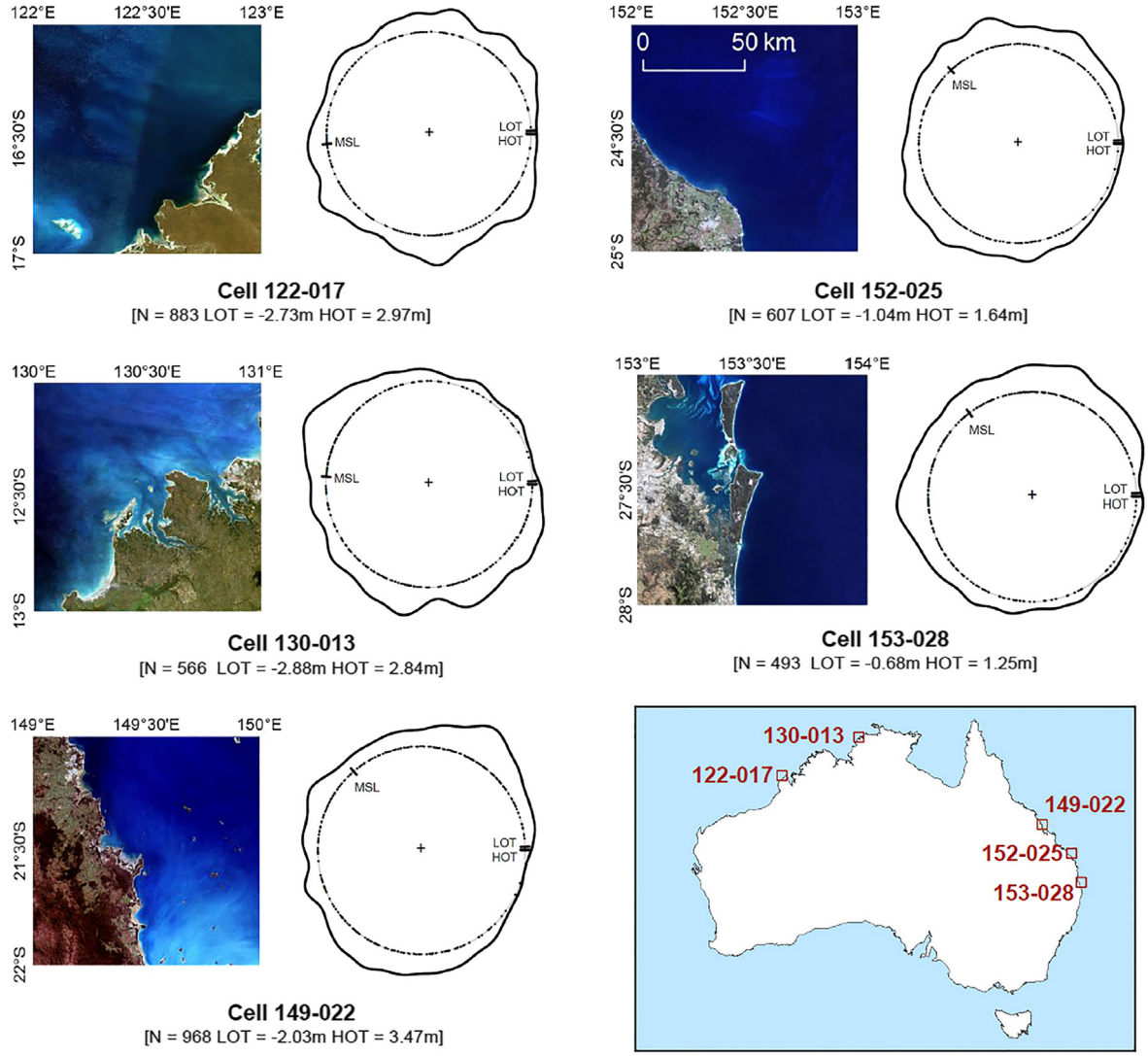

Fig. 5. Overview of Case Study Sites – locations of the five study sites used for assessment of the model examples shown in this paper. The number of tile observations (N) and values for lowest observed (LOT) and highest observed (HOT) tides are also shown. The circular plots display the density and distribution of tile observations across the OTR for each study site, calculated using a Von Mises kernel density estimator (bw = 100).

al., 2013; Roy et al., 2010), medoids (Flood, 2013), and parametric scoring (White et al., 2014), seek to create a composite with pixel values most representative of the full ensemble, unaffected by noise or outliers in the data.

In our situation we have the simpler case that we are dealing with single-band images of NDWI values and compositing can be viewed as constructing an estimate of the most representative value at each pixel of the observations within one of our tidal intervals. We achieve this by taking the median of the NDWI values at each pixel through the ensemble of NDWI images in each tidal interval. The median is a highly attractive approach due its well-understood behaviour.

Using the median allows us to circumvent a number of potential problems with the tile observations which include: (1) data gaps from artefacts such as Landsat 7 Enhanced Thematic Mapper Plus (ETM+) Scan Line Corrector (SLC)-off gap striping; (2) residual noise and confounding factors not captured by pixel quality flagging (e.g. cloud edges and cloud shadow); (3) temporal random variations that may affect individual NDWI values. For example, the variation in spatial distribution and extent of remnant water on tidal flats between ebb and flow tide (Ryu et al., 2002), or breaking water over shallow areas and reef crests that may result in misclassification (Dhanjal-Adams et al., 2016).

The fundamental assumption in our method is that by partitioning the tile observations into intervals of the tidal range, we are observing similar exposed intertidal extents throughout the subset ensemble of images. Whilst the median deals with outliers and noise in the interval ensemble, we need to test this underlying assumption. This is done by calculating the within interval variance of the NDWI values at a pixel level, and combining them to derive an average interval based NDWI variance image for each cell (Fig. 3). This acts as a confidence layer tool that can allow us to examine where our assumption may not hold (for further discussion see Section 4.2) and to compare it against the asymptotic theory for the sample median (see Appendix A).

3.3. Creating a topographic model

To create the relative extents model we first derive binary water/non-water images from the nine NDWI composite images for each coastal cell. This involves determining a threshold for NDWI values to delineate between water and land. It is noted that the NDWI threshold can vary between images (Liu et al., 2012), and thus manual adjustment of the threshold on an image by image basis is often performed (Dhanjal-Adams et al., 2016; Murray et al., 2012). In practice, this is

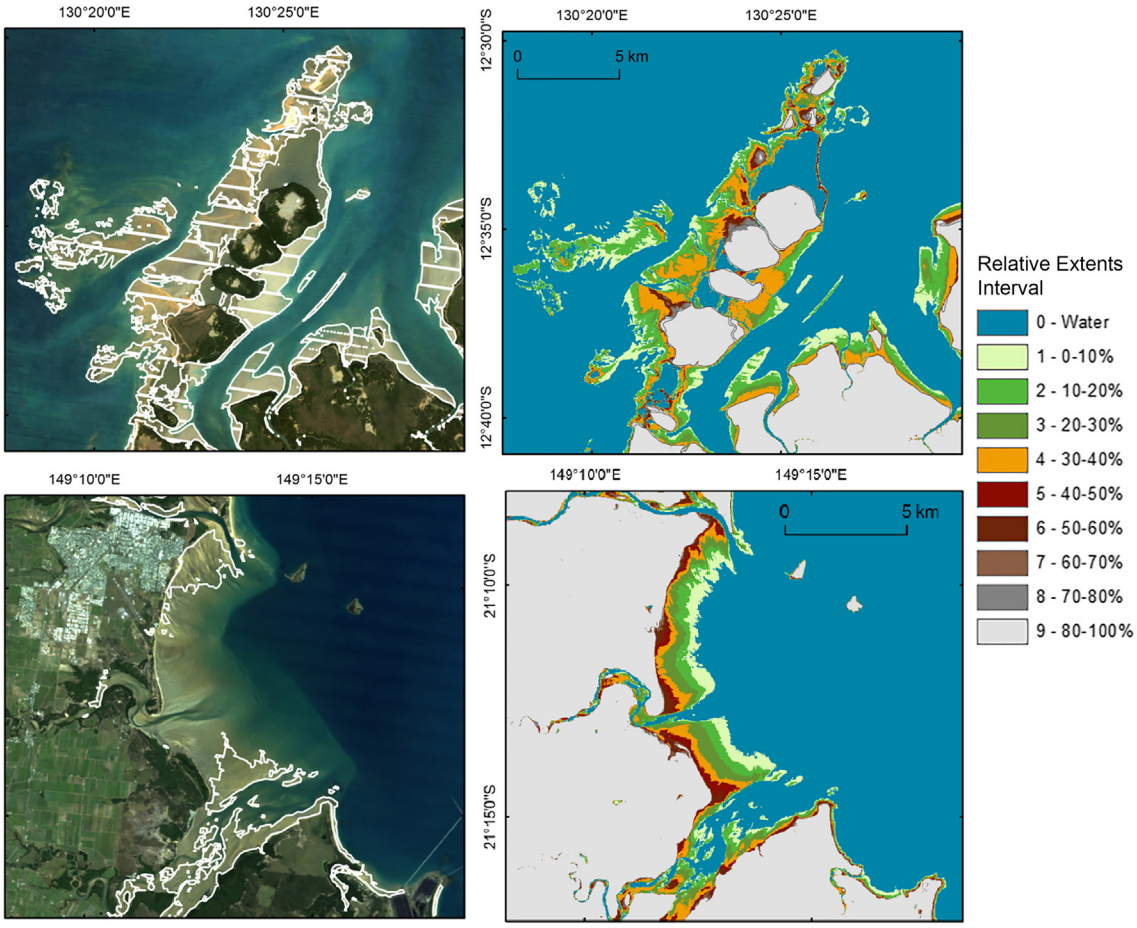

Fig. 6. Comparison to a Paired Single Scene approach – the derived relative extents model (right) for sections of Cells 130-013 and 149-022, shown in comparison to the national scale extents model (white boundary) produced by Dhanjal-Adams et al. (2016). Note the topographic detail derived by the relative extents model, without data gaps or artefacts evident in the paired scene model.

feasible (yet time consuming) for continental scale studies such as Dhanjal-Adams et al. (2016) which only used 99 image pairs to cover the Australian coastline. For our study, the manual thresholding approach is not practical for all 1989 median composites over the time-series.

There are a number of recent studies noting that the use of well calibrated surface reflectance data, such as NBAR, can assist in threshold standardisation for water indices (Feyisa et al., 2014; Fisher et al., 2016; Liu et al., 2012). In their study on the radiometric correction influence on these thresholds, Liu et al. (2012) found that the average NDWI threshold when moving from digital number (DN) to surface reflectance trended towards zero, moving from 0.15 to 0.017. They also found 90% of the variability in threshold came from temporal influences such as sun/sensor geometry and atmospheric effects; which are accounted for in the NBAR atmospheric correction.

Considering these findings, and the practical constraints of the number of observations in our time series, we implemented a zero threshold to derive the binary images for each of the derived median NDWI composite layers. The application of a standardised threshold to a composite index image is fundamental to our stated objective; to develop an automated and consistent methodology.

The thresholding process results in nine binary images for each of the 221 cell locations, representing the extent of water/non-water at each interval of the OTR. To create the relative extents model, these nine layers are combined, producing model values ranging from zero to nine. These integer values reflect the extents of exposed substratum modelled at each percentile interval of the OTR. Zero values indicate regions always covered in water; values of 1–8 represent the exposed extents at 10% intervals of OTR from the lowest 0-10th percentile through to the 70-80th percentile, with a value of 9 indicating land areas still exposed at the highest 80-100th percentile of the OTR. This process of analysing spatial extents based on tidal intervals enables us to not only model the extents of the intertidal flats, but also the relative topography of the zone (Fig. 4).

3.4. Assigning elevation values

To test the concept of generating an elevation model from our continental scale extents model, we selected two cell locations (Darwin Harbour, NT and Moreton Bay, QLD) with available in-situ elevation data in the intertidal zone. We note that creating an absolute elevation model is not the primary aim of this study. However, by acknowledging and considering the influence of our median composite and tide modelling process when validating these models, they provide further information on the application of our method and inform on directions for future work.

To assign elevation values and create a continuous digital elevation model (DEM) for each cell, we first derive waterline contours at the boundaries of each of the exposed extent intervals in the relative extents model. Utilising the OTPS model to assign tidal heights relative to MSL allows us to attribute not only the upper and lower extents of the OTR, but also to determine the corresponding median tidal height for each tidal interval ensemble in the model. These values are then used to assign an elevation value to each of the derived contours.

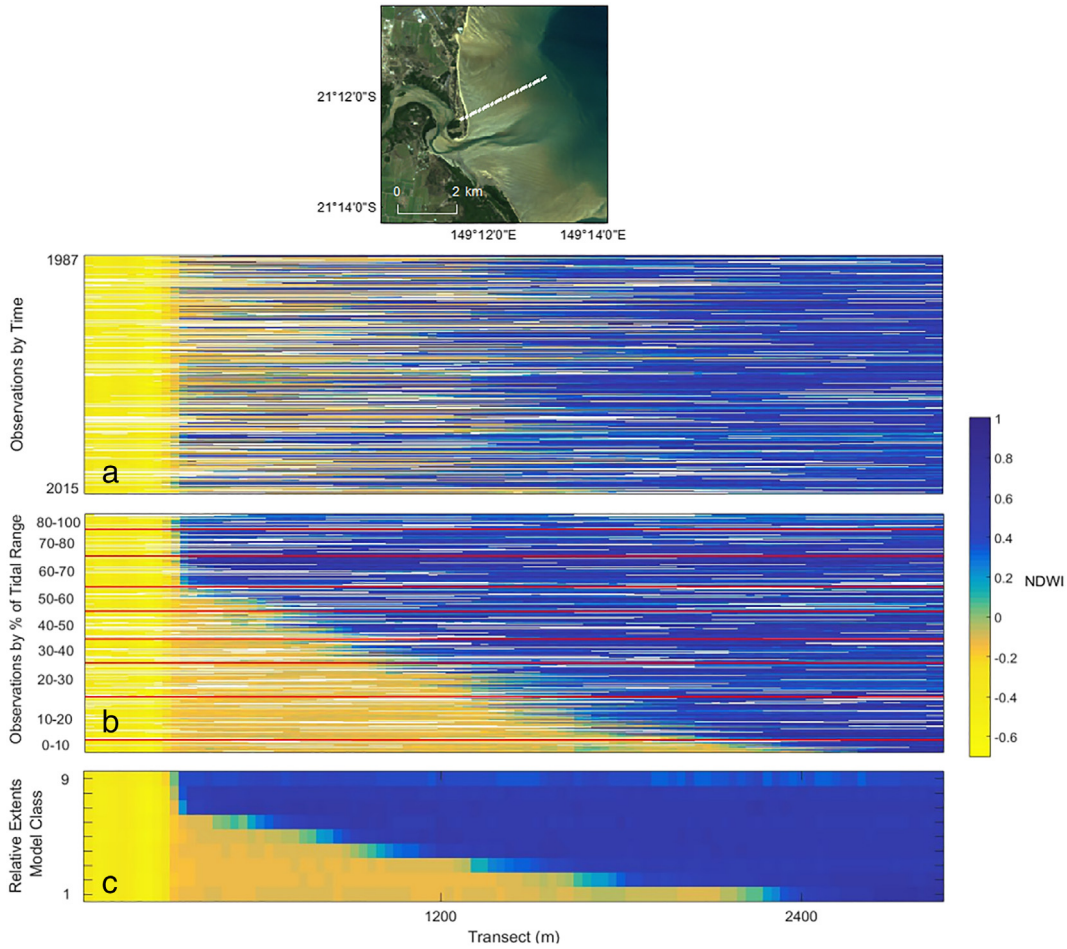

Fig. 7. Hovmöller analysis of the Relative Extents Modelling process – the full ensemble of NDWI observations derived from a transect at Mackay, QLD (Cell 149-022) ordered by date/time of acquisition (a). The ensemble is reframed into an alternate domain ordered on attributed tidal height, and partitioned into intervals of the observed tidal range (b). Median composites are then generated for each tidal range interval (c), effectively dealing with the data gaps and noise evident in the full ensemble.

The contours are used to create a triangulated irregular network (TIN) model utilising linear interpolation of the MSL elevations, implemented within the ArcGIS 3d Analyst toolbox. The choice of interpolation using the TIN model was based on the ability of the method to define and maintain the waterline contours as breaklines in the model. The elevation values of the TIN are mapped back to the original pixel resolution of the relative model to create a cell-based DEM of the intertidal zone; the breaklines of the TIN ensuring the location of the original contour elevation values are maintained in the underlying pixels.

To estimate the uncertainty of the derived DEM we use the distribution of the tidal heights for each interval ensemble of observations. The standard deviation of the attributed heights within a given interval is assigned to each of the elevation pixel values, based on the spatial extent of the interval in the relative extents model. This uncertainty value provides an indication of the variability of tidal heights within each interval that the median elevation values are drawn from. As such, it is an estimate of the uncertainty of the values as a function of the DEM process implemented; rather than an uncertainty based on the physics and attribution characteristics of the OTPS tidal model itself.

4. Results

4.1. Continental scale relative extents model

The development of a consistent and automated workflow enabled us to generate a continent scale intertidal relative extents model for the full Australian coastline, analysing an average of 859 Landsat observations at each of the 221 cell locations. To illustrate the benefits of our time series approach, and the application of the confidence layer and derived elevation models, we have chosen five locations across Northern Australia with a significant tidal range and intertidal zone extent (Fig. 5).

The ability to query the full time series of observations at any location is a significant shift away from individual scene analysis. The median compositing approach employed across tidal intervals enables us to create a continuous model across regions where previous single scene methods have been restricted by sensor artefacts and/or clear, cloud free data availability at the low and high tide extents (Fig. 6). This restriction is acknowledged in the national scale model produced by Dhanjal-Adams et al. (2016), with particular reference to ecologically significant regions such as Roebuck Bay and the Kimberley Coast in Western Australia, which the authors were unable to map due to the lack of high quality single scene imagery.

Through shifting the analysis away from a traditional time-series, and mapping the observations to the modelled tidal height, we are able to interpret, query and model the pixel based NDWI values in a completely different manner. This concept is well illustrated by examining a single transect across the tidal flat at Mackay, Queensland (Fig. 7). Hovmöller plots such as this are commonly used to examine profiles of data, to visualise the spatial evolution of the variable in question over time (Hovmöller, 1949). Under this traditional paradigm (Fig. 7a), it is clear the spatial variations of the NDWI values are not driven by time, but by the tidal height at which each observation is acquired. Thus, the extents of the individual observation profiles are randomly distributed, as the sun-synchronous satellite observes at different tidal stages through time. This is illustrated in the circular plots of observation density distributed across the OTR shown in Fig. 5.

By ordering the observations based on their attributed tidal height, we can observe a much more coherent relationship, with the expected trend towards an extended spatial profile of low NDWI values as the tide height decreases (Fig. 7b). This visual representation also illustrates the rationale behind the previous decision made to merge the upper 80–90% and 90–100% ranges of the OTR, both in terms of spatial extent and sample size. Partitioning the tidal series of observations and applying the median compositing approach (Fig. 7c) then allows us to deal with two other aspects of data noise and uncertainty that are well illustrated by displaying the data in Hovmöller format.

First, within each tidal height partition there is still variation in spatial extents of the NDWI values that do not correspond exactly with the order of the attributed tidal heights. There are a number of possible reasons for this, based on the environment and our modelling process. Natural variations in the spatial location of the waterline are often observed under similar tidal heights on low gradient tidal flats (Li and Gong, 2016) as is the extent and location of remnant water under ebb and flow tide conditions (Ryu et al., 2002). In a modelling context, any local inaccuracies driven by the scale of the tidal model and the relative location of the single modelled tidal post location will also contribute to a variation across the partition (Liu et al., 2013; Bell et al., 2016), as will the sensitivity to different environmental and seasonal factors such as turbidity (Liu et al., 2012; Mason et al., 1997; Ryu et al., 2008).

Second, it is evident that missing data and, in a pixel quality context, noisy data is not perfectly captured in the pixel-quality masking stage. To utilise the full time series, gaps in each observation across the tile footprint (from partial scene coverage, SLC off-gaps, etc.) are treated as no data, and can be seen represented as the white sections through the Hovmöller plots of Fig. 7a & b. Similarly, the pixel quality process masks clouds, cloud shadow or saturated pixels for each tile. The extent of the data gaps for this single transect illustrates the difficulty in selecting single scenes for analysis, particularly at the extents of the tidal range where observations are less frequent. Compounding this issue is the effectiveness of the pixel quality procedure. For example, pixels at the edges of clouds or very thin cirrus or haze type clouds may be missed in the cloud masking process. Alternatively, bright targets such as sand or salt pans can be misclassified as cloud (Zhu and Woodcock, 2012), resulting in further missing data in the single image context.

Partitioning the observations and performing a pixel composite using the median allows us to leverage the full time series of data, including observations with these significant data gaps that would be discarded in other applications. Outliers within the partition ensemble from uncaptured noisy data are disregarded, and the variations in NDWI from natural and/or modelling influences are accounted for and contribute to a representative pixel based median NDWI at each tide height partition (Fig. 7c). This allows an automated process for creating smooth, continuous NDWI composites for each tidal stage, feeding into our relative extents modelling at a continental scale.

The tidal interval partitioning also allows us to examine the application of our consistent zero thresholding of the NDWI composites in our methodology. As we have discussed, for an automated continental workflow, manual thresholding based on visual inspection is not feasible. There have been some recent attempts to derive automated thresholds. For example, subsetting the data to localised regions to enable balanced sample sizes, that are in turn analysed using the Otsu thresholding algorithm (Donchyts et al., 2016). Although that approach enables the image-based environmental variability to be accounted for, our composites are derived from an ensemble of images under different environmental conditions (e.g. ebb/flow tide), hence their method is not strictly applicable and difficult to implement at a continental scale. To illustrate this point and to compare it to the performance of our zero threshold in the context of the ensemble, we completed the Otsu thresholding on a single tidal interval ensemble of images for the Mackay image used for Fig. 7. Based on that ensemble of images, we mapped the extent of the optimal waterline locations derived, and show that our zero threshold waterline obtained from the median NDWI composite falls within that range at all points (Fig. 8). Importantly, it also shows the consistent threshold approach to estimate a waterline location within the range of the optimised waterlines for the ensemble of images, any one of which would be deemed suitable (before consideration of noise or data gaps) for single scene analysis under the lowest 10% of tides methodology of previous continental scale applications (e.g. Dhanjal-Adams et al. (2016); Murray et al. (2012)).

4.2. Evaluating tidal range interval ensembles

Underpinning our method is the assumption that the OTPS tidal model (and the way in which we have implemented it) allows us to successfully order and partition observations into bins of the OTR, and that the variations in water/not water observed are driven by tidal influences. This has two practical implications as we move the analysis away from the time domain.

Firstly, as we group observations based on tide, the implicit assumption is that the environment we are modelling is not changing over time.

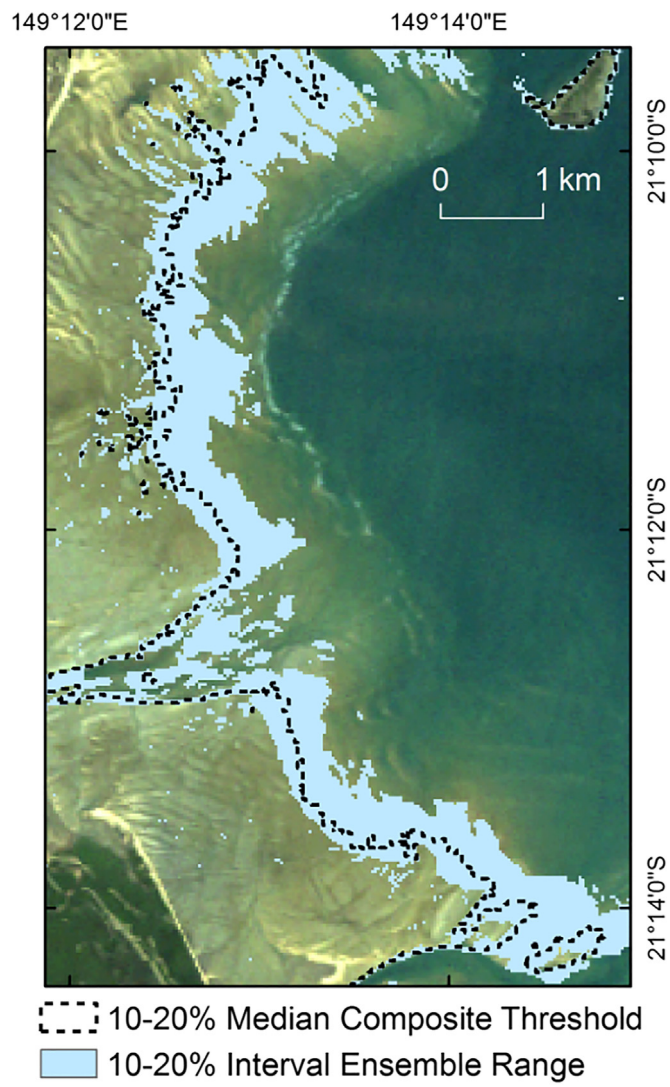

Fig. 8. Implementing a standardised threshold for the NDWI Median Composite – the location of the zero threshold waterline for the 10–20% tidal interval NDWI median composite at Cell 149-022. The standardised threshold is shown in comparison to the full range of waterline positions derived from an optimised NDWI thresholding (see Donchyts et al. (2016)) of each of the 156 individual observations in the 10–20% tidal interval ensemble.

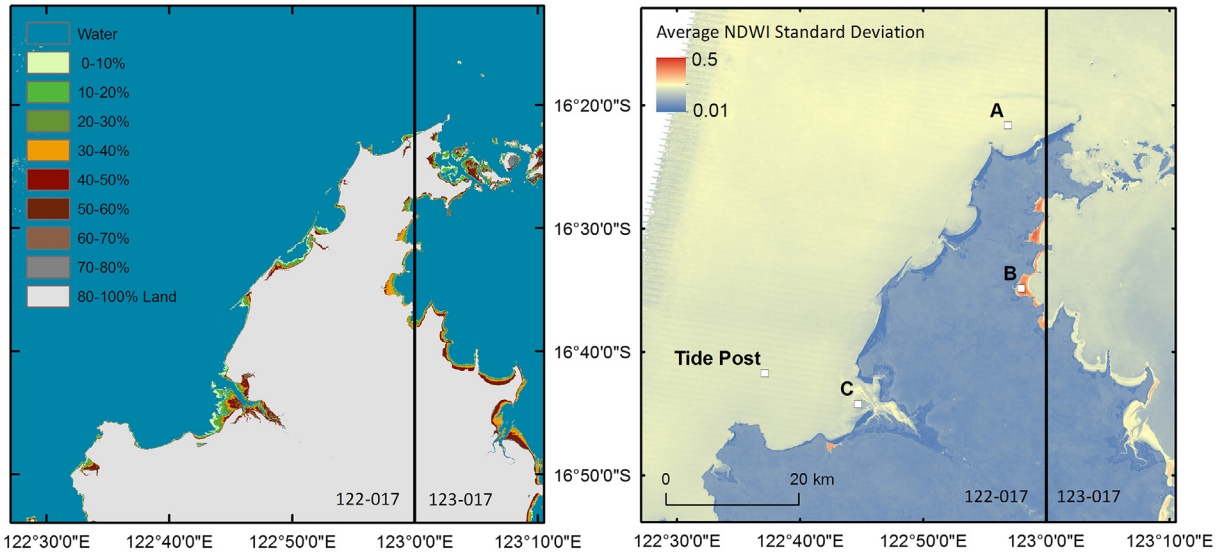

Fig. 9. OTPS modelling errors and the Confidence Layer – the Dampier Peninsula, WA (Cell 122-017), illustrating OTPS tidal attribution errors introduced by complex coastal features and the cell based architecture of the AGDC. Note the location of the cell boundary and representative tidal post of Cell 122-017. The Confidence Layer (right) highlights the region on the eastern boundary of the cell, indicating that the tidal heights modelled at the tide post do not correspond to the pattern of water/not-water observed in this area.

Second, we assume that that the OTPS modelling process we are using accurately defines our new tidal height domain.

In a dynamic and complex coastal environment, it is unlikely that both these assumptions will hold in all locations. As we have shown in the Hovmöller visualisation, there is already uncertainty and variation in the model, even when the trend maps broadly to the tidal height domain. The question then becomes, what happens when the tidal domain assumptions and modelling conditions are clearly contradicted?

To assess this we use the confidence layer tool described in Section 3.2.2, which evaluates the pixel based variance of the ensemble of NDWI observations within each partition. In concept, this is similar to the method employed by Bell et al. (2016) who used the correlation of SAR pixel intensity with the modelled tidal height across a time series to indicate regions which were intertidal in nature. There are differences to our approach; firstly the NDWI values do not map as continuously and consistently to wetting and drying of a pixel as SAR intensity returns, hence we use within tidal interval variance as an indicator of behaviour corresponding to tidal height. Secondly, we are interested in highlighting regions where errors in our modelling assumptions occur, not in defining the intertidal zone itself.

To illustrate the use of the confidence layer in a scenario where errors are generated by the tidal modelling process, we examine a location on the Dampier Peninsula, Western Australia (Fig. 9). In this region, the area highlighted by the confidence layer exists on the eastern side of the peninsula, at the extents of the AGDC cell. The use of single tidal post location means the representative tide post for this cell is located on the western side of the peninsula, separated from the area of interest not only by the peninsula, but also a complex network of islands and onshore reefs east of the tip of the peninsula. The influence these structures have on the modelled tide at the eastern shores of the peninsula is evident in the increased variance modelled in the confidence layer, and whilst this an extreme example based on the location of the AGDC cell boundary, it clearly indicates the influence of the complex coastline over simple distance from the modelling location (Fig. 10).

The confidence layer highlights this error by examining how well the tidal heights modelled at the tidal post explain the variation we observe in NDWI values at Site B. We can contrast this with the variation seen at Site C, at an intertidal flat close to the tide post. We observe that when mapped to the time domain, both points show a random distribution of NDWI values, characteristic of an intertidal flat

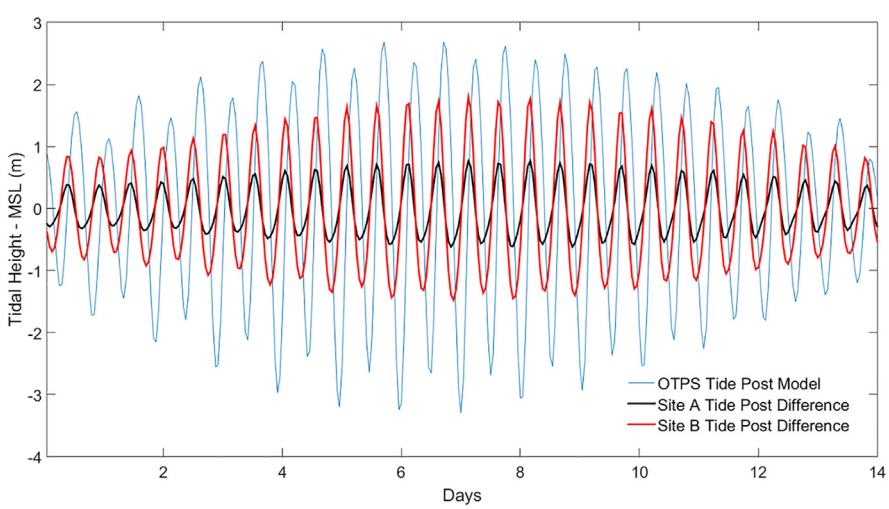

Fig. 10. Comparing the influence of distance and coastal structure on OTPS modelling - difference between the modelled OTPS tidal height at the tide post of Cell 122-017 and the heights modelled at Sites A and B over a 14-day period. Site A is a further straight line distance from the tide post than Site B, however Site B is located on the opposite side of the Dampier Peninsula (Fig. 11). The larger difference in modelled heights at Site B indicates the increased influence of the complex coastline on the spatial variation of the OTPS model.

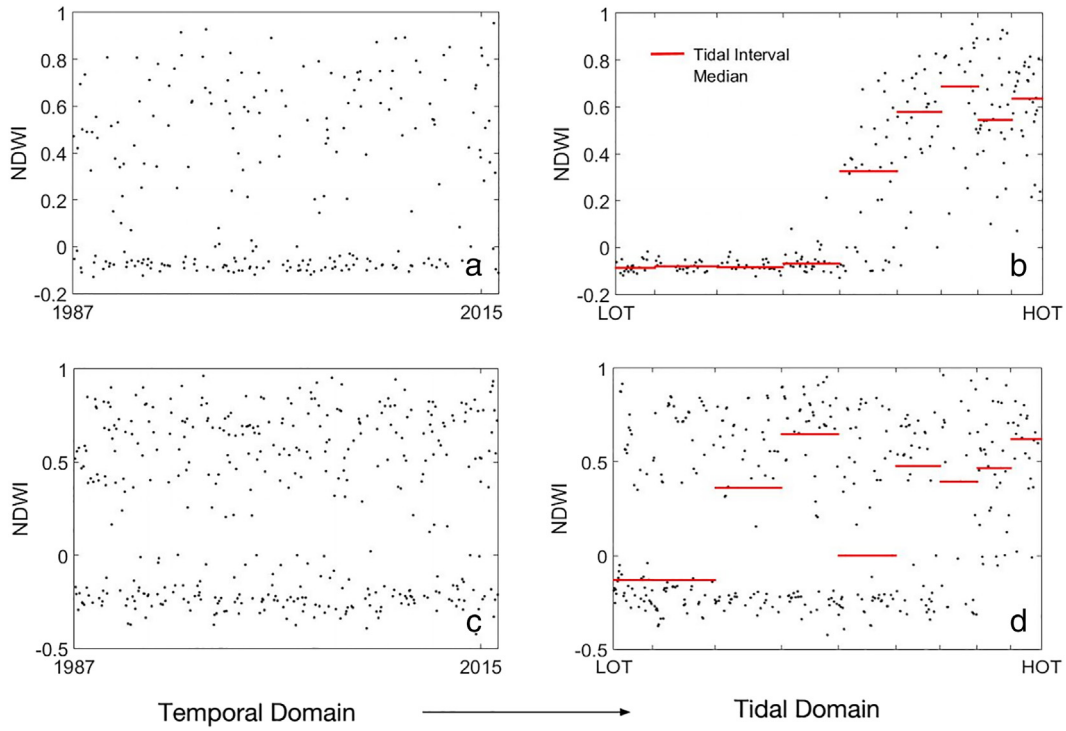

Fig. 11. Examining errors in the tidal model by shifting from the temporal to tidal domain – examples of NDWI Observations at Dampier Peninsula pixel sites, Cell 122-017 (see Fig. 9). a) Site C - NDWI by Time, b) Site C – NDWI by Tide, showing derived median NDWI values at tidal intervals, c) Site B – NDWI by Time, d) Site B – NDWI by Tide, showing derived median NDWI values at tidal intervals.

(Fig. 11a & c). There is a marked difference when we then map to the tidal heights modelled at the tide post. At Site C we see a clear pattern of exposed negative NDWI values at low tide, moving to inundated positive values as the tide height increases (Fig. 11b). In contrast at Site B, we see that the tide heights explain no more about the NDWI variation than the observation time (Fig. 11d). Hence, this is reflected in the confidence layer as an increased variance across each of the tide height intervals. The consistency of values within tidal intervals at Site C enables us to infer meaningful median values (Fig. 11b) and shift the analysis to the tidal domain, in comparison to the unordered median values derived at Site B (Fig. 11d).

In the second scenario, we examine how the confidence layer deals with a situation where the geomorphology of the coastal environment has changed over time (Fig. 12). In these two dynamic coastal locations we see different types of coastal change. At the south-east extents of Moreton Island we see the formation of a sand spit, followed by a pattern of erosion and deposition over time as the spit erodes and the beach profile increases at the south-west corner of the island. In the second example, we see the complex sandbar structures at the mouth of Burnett River shifting significantly over time, with the estuary almost completely closing to the ocean through the time series. The images shown in Fig. 12 are only three snapshots of the time-series, and in the confidence layer we are able to model the full extents of these regions of coastal instability.

To demonstrate how the confidence layer responds to this type of coastal or estuarine change, we examine the behaviour of the NDWI values over both the temporal and tidal domain (Fig. 13). By comparing a location where change can be observed over time (Site A in Fig. 12),

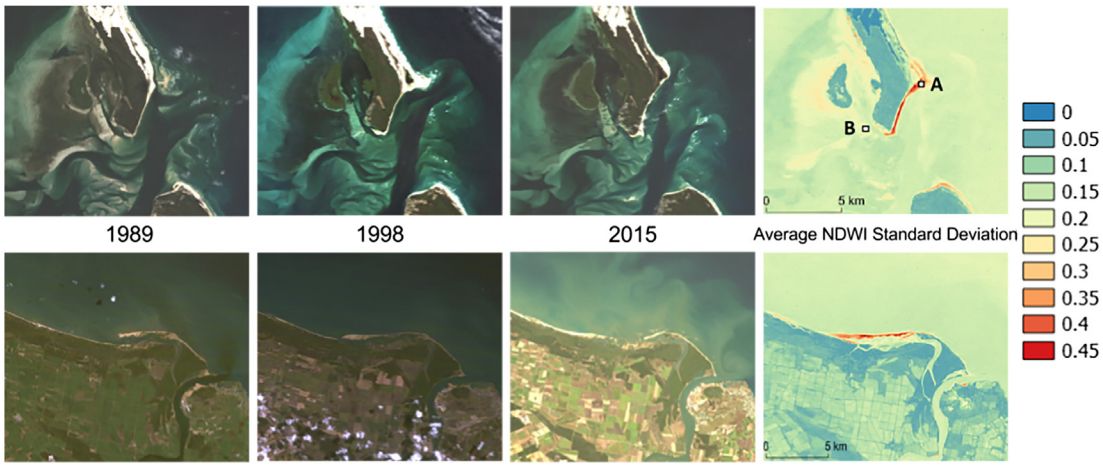

Fig. 12. Coastal stability and the confidence layer – time series image observations showing coastal change over time at the entrance to Moreton Bay, QLD (cell 153-028) and the mouth of the Burnett River, QLD (cell 152-025). These areas of change are reflected by increased values in the confidence layer, corresponding to the average within tidal interval standard deviation of NDWI values. Sites located in regions of high variability indicating coastal change (A) and lower variability in the intertidal zone (B).

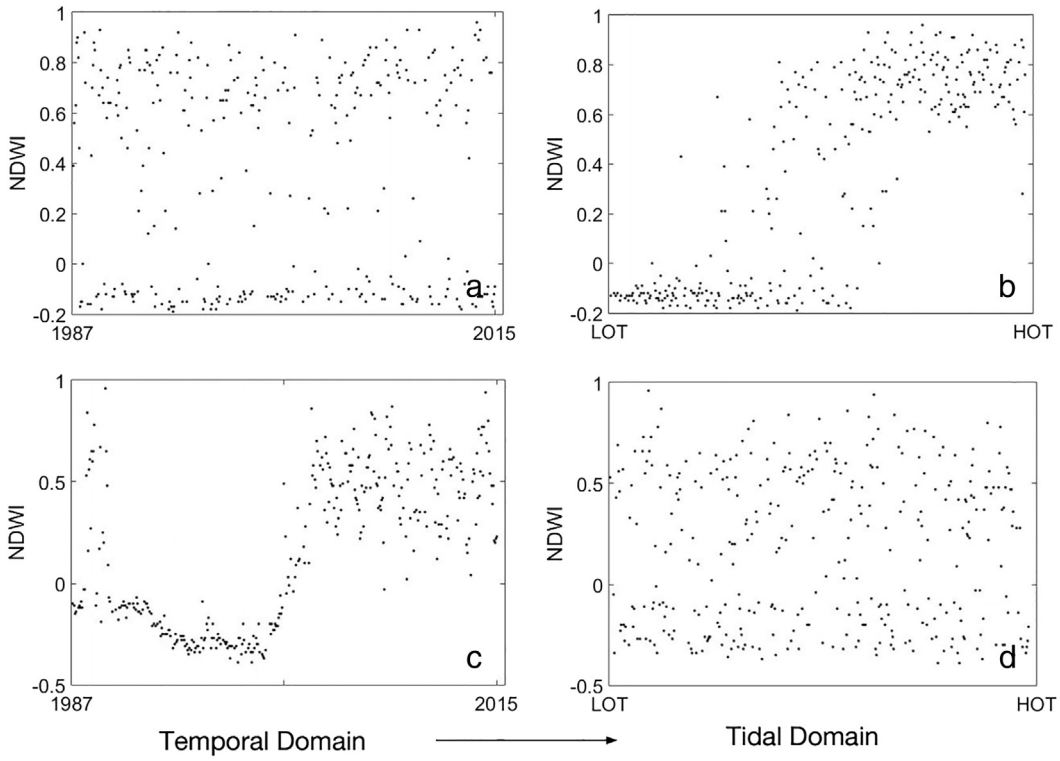

Fig. 13. Examining coastal stability by shifting from the temporal to tidal domain – examples of NDWI Observations at Moreton Bay pixel sites, Cell 153-028 (see Fig. 12). a) Site B - NDWI by Time, b) Site B – NDWI by Tide, showing a response pattern to tide heights, c) Site A – NDWI by Time, showing a response pattern over time, d) Site A – NDWI by Tide.

with an intertidal location (Site B in Fig. 12), the series of NDWI observations gives an understanding of what drives the pattern of wetting and drying at each point. When sorted over time the standard random tidal response is observed at Site B (Fig. 13a), whilst at Site A the geomorphological change that occurs as land forms and then erodes at this point is clearly highlighted (Fig. 13c). Switched to the tidal domain, we see the pattern of dry to wet as the tide height increases at Site B (Fig. 13b), whilst Site A remains random and highly variable across the full tidal range (Fig. 13d).

In summary, the confidence layer provides a mechanism for evaluating the assumptions fundamental to the reframed tidal domain analysis of our method, and therefore a tool to assess the quality and relevance of the relative extents model. From a spatial perspective, our method depends on the tidal attribution's ability to partition observations successfully into intervals of the tidal range. From a temporal perspective, the method assumes patterns of water/non-water classification to be driven by tidal influences. Hence, when the ensemble analysis is reframed into the tidal domain, the confidence layer can identify pixels and regions where these assumptions do not hold, and where the extents model should be interpreted with caution.

4.3. Case study assessment of elevation model

To evaluate the potential for generating intertidal elevation models using the approach described earlier, digital elevation models were produced for AGDC cells 153-028 and 130-013, encompassing Moreton Bay, QLD and Darwin, NT respectively. Sites within each of the cells were selected based on the availability of validation data, and on the proximity to the location of the modelled tidal post location for the cell.

We acknowledge that the accuracy of the derived DEM is likely to decrease the further we are from the tidal post location, or with increased complexity of the coastal environment. Thus, validation of the sites in this section is intended as a feasibility assessment of using our automated modelling framework to derive an elevation model; with the associated challenges of scaling up to a full DEM creation discussed further in Section 5.

4.3.1. Validation sites and RTK GPS data

Real Time Kinematic (RTK) GPS transect elevation data was collected and processed for the intertidal flats of Moreton Bay, QLD at spring low tide as detailed in Danaher and Collet (2006). Data was processed to Australian Height Datum (AHD) elevation, with a stated horizontal accuracy of 0.02 m and vertical accuracy of 0.03 m.

Transects from these data were selected at two locations in the south-eastern extent of the Bay (Fig. 14). Both transects incorporate the full spatial range of the derived DEM from highest to lowest observed tide, with a horizontal point spacing in the range of 15-40 m.

Elevation data for the Darwin Harbour model validation was acquired on tidal flats of East Point, at the southern extent of Mindal Bay, NT (Fig. 15). The data was acquired via an RTK GPS survey conducted by HydroSurvey Australia as part of the broader bathymetric and topographic survey of the region detailed in HydroSurvey Australia (2009). Data was processed to AHD elevation, with a stated horizontal RMS accuracy of 0.01 m and vertical accuracy of 0.02 m.

The full data set consisted of 2793 point observations (Fig. 15a) corresponding to the extents of the derived DEM for cell 130-013, at a horizontal spacing of 2-3 m. A specific transect was also extracted (Fig. 15b) at the Eastern extent of the survey area for comparison to the DEM data.

4.3.2. Validation results

Both DEM transects in Moreton Bay (Figs. 16 and 17) show a strong general agreement with the GPS data, with associated uncertainty in the model encompassing the validation offset in the majority of locations. One of the major differences we observe is an overestimation of elevation at 200 m to 400 m in Transect A. This feature is an illustration of the sensitivity of this type of validation to not only the resolution of

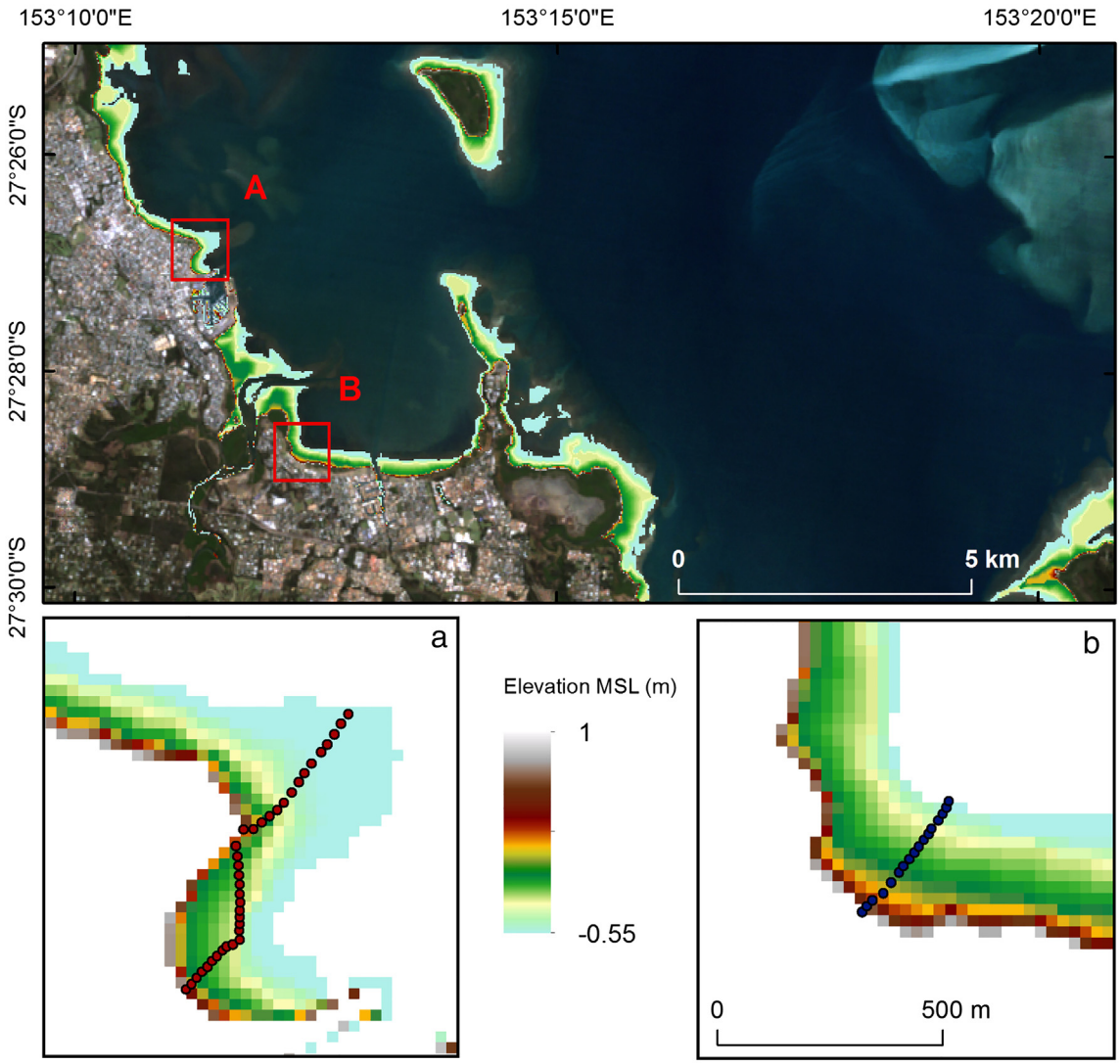

Fig. 14. Moreton Bay (Cell 153-028) DEM and validation sites – transect sites A and B shown overlaid on the derived digital elevation model.

the DEM model, but also the georeferencing accuracy of both the underlying imagery data and the GPS observations. The overestimated section occurs in a region where the transect turns and runs in parallel to the coastline (see Fig. 14a), with the transect points running along the eastern edge of the pixels in this location. A shift of 4 m to the east in the DEM into the next column of 25 m pixels would estimate an elevation of −0.44 m, closer to the validation data.

Where the transect runs perpendicular to the coastline along with the elevation profile of the tidal flat, such as shown in Fig. 17, we see a much closer match to the validation data. Of note is the under and overestimation of the model at the highest and lowest extremes of both transects respectively. This may be a result of the central estimation of the median heights in each of the tidal interval partitions. As shown in Table 2, not only do we observe a portion of the full tidal range, but the median estimator further reduces the range as applied to the elevation model. Hence, the uncertainty associated with this median estimation (shown as the grey range in the transect validation figures) is useful when assessing the model.

The issue of model resolution is clearly seen in the Darwin Harbour validation results. The GPS data acquired at East Point is of a much higher spatial resolution (~3 m), mapping the fine scale elevation features. Some of these features are inevitably smoothed out in the 25 m pixel resolution of the inter-tidal DEM. Spatial resolution artefacts are likely to produce some of the validation outliers seen in Figs. 18 and 19. Taking this into account, comparison of the low resolution DEM to the higher resolution RTK GPS data yielded an R^2 value of 0.57, and a mean absolute height difference of 0.57 m.

Given the automated, continental-scale method we have employed, we consider that these validation results show the considerable potential of the model outputs to be translated into an intertidal DEM product. Crucial to this potential is improving the local accuracy and characterising the spatial variation of the tidal model, whilst still maintaining the capability to model at a continental scale.

5. Discussion and future directions

The ability to utilise the full time series of earth observation data; at a continental scale, underpins the fundamental concepts and benefits of our method. By removing the dependency on high quality single scenes at appropriate acquisition epochs we have been able to create a continuous model, in regions where previous single or paired scene analysis has failed. There are two core concepts that enable our method to achieve this scale of temporal and spatial analysis.

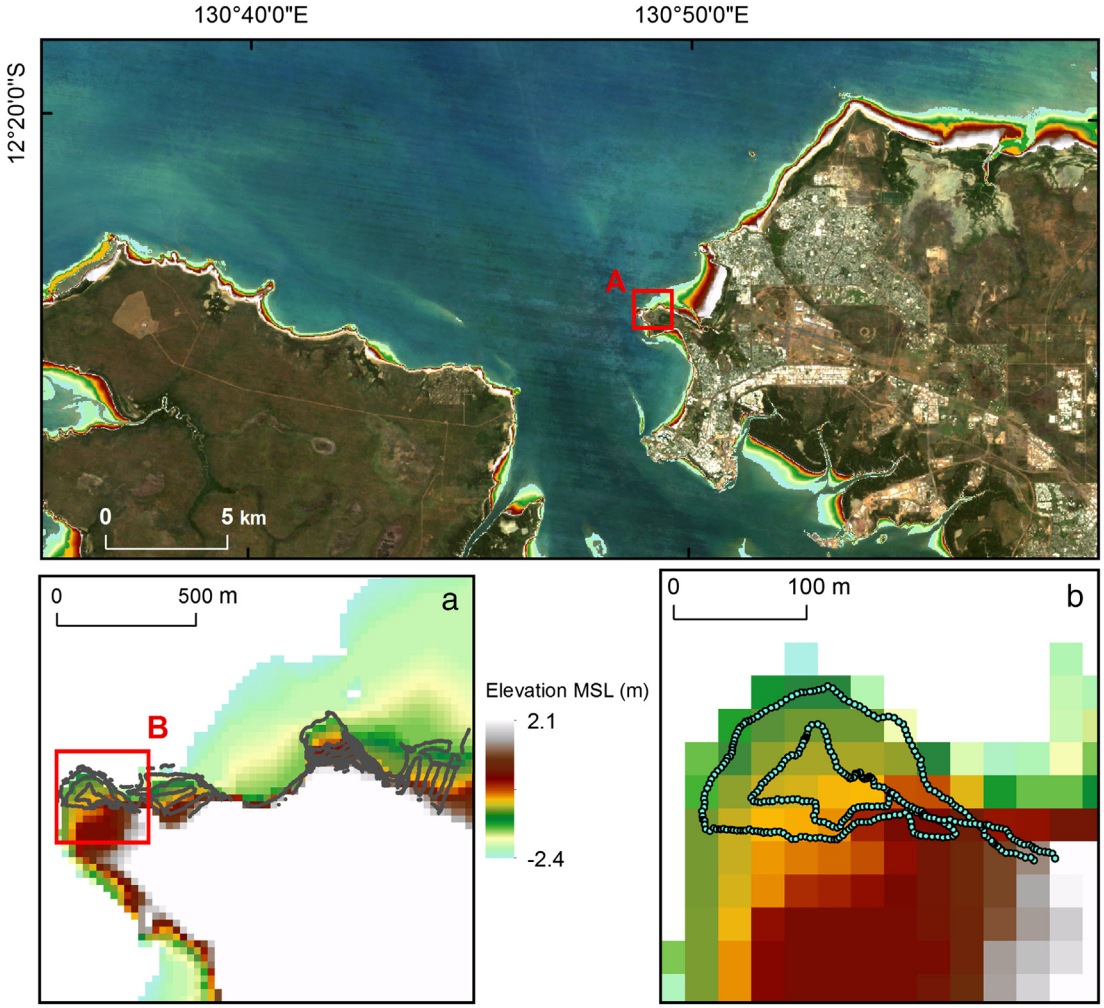

Fig. 15. Darwin Harbour (Cell 130-013) DEM and validation sites – full RTK GPS survey (A) and East Point Transect (B) shown overlaid on the derived digital elevation model.

Firstly, the development of an automated process that minimises subjectivity and manual interpretation was critical to allow the full time series of data to be analysed. With an automated process there are generalizations that must be made, along with the uncertainties in both the data and modelling process that must be accounted for. The median compositing method we have described has been shown to be effective in dealing with a range of these issues. The statistical robustness of the median is particularly useful in pixel based analysis to account for data gaps and noise across the time-series, allowing for unavoidable inaccuracies in pixel-quality or masking processes and variations in data coverage and quality. We have also shown that applying the median composite to an ensemble of NDWI outputs can assist in dealing with the uncertainties in both the tidal model and NDWI thresholding process. By discarding outliers in both these processes across a tidal interval, a robust central measure is returned, enabling a standardised approach across the continent. When the underlying

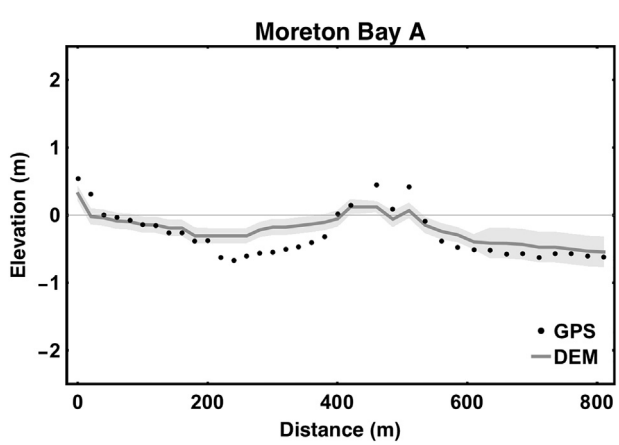

Fig. 16. DEM validation for Moreton Bay Transect A – DEM uncertainty range of ±1.96σ shown in grey.

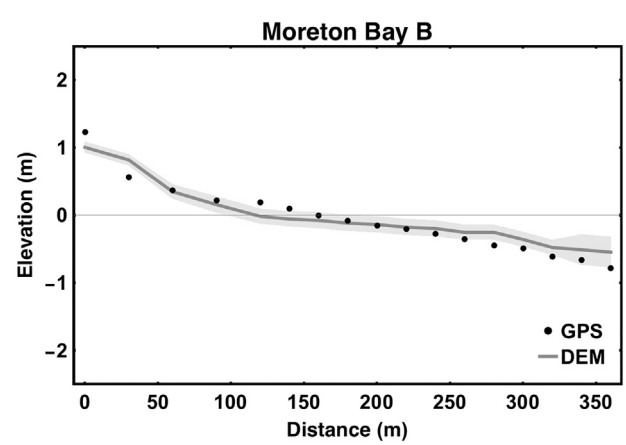

Fig. 17. DEM validation for Moreton Bay Transect B – DEM uncertainty range of ±1.96σ shown in grey.

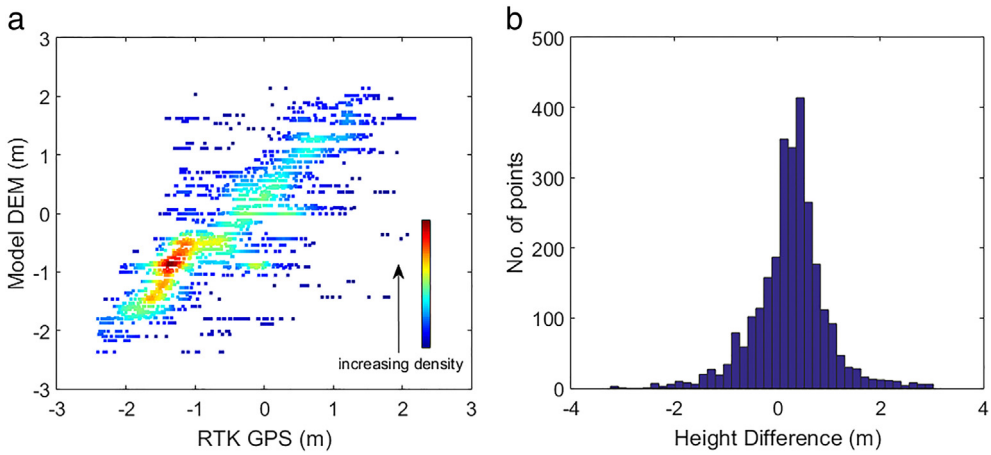

Fig. 18. Comparison of the derived Darwin Harbour (130-013) DEM to the full RTK GPS survey – density scatterplot (left) and histogram of height differences (right).

assumption of similarity within a tidal interval is violated to a point where the median approach is unable to accommodate, this variability is captured and highlighted in the confidence layer.

Modelling the median of ensembles at each extreme of the tidal range, it would be reasonable to expect that the derived tidal zone extent of our model would not cover the full range of a single scene analysed at the lowest (or highest) tide possible. Whilst this is no doubt the case in some regions, we have observed favourable extent coverage in many areas of the model when compared to the model of Dhanjal-Adams et al. (2016), along with the noise reduction benefits of the median (see Fig. 6). This may be due to the difficulty of mapping the waterline on gently sloping tidal flats, where Li and Gong (2016) noted variations of the horizontal position estimated on similar tidal heights, even with supervised classification and thresholding. Within a tidal interval, the median is again an effective tool for dealing with this variation.

The second key concept is that of reframing the time-series analysis away from the temporal, and into an alternate (tidal height) domain. By shifting the analysis in this way, we not only enable the tidal height based median analysis, but open up new ways to interpret the data. The confidence layer was designed to highlight where modelling or data variability compromised our extent modelling process, however it has shown an additional capability to identify areas of change and coastal instability. Exploring how to isolate these change detection capabilities and additional methods for leveraging this shift between ensemble domains is a key for future work on the model.

Whilst the choice of a standardised NDWI threshold is supported by the calibrated nature of the reflectance data and mitigated by the median approach, we recognise that exploring an automated threshold method (and other relevant indices) may help to reduce the uncertainty in this step of the process. A region based optimisation of the threshold, such as that implemented by Danaher and Collet (2006), may be relevant, as it could still be applied to the median composite of our process. Their optimisation is achieved through the regression and ranking of water area mapped vs tidal height, and is dependent on the accuracy of the tidal height attribution method.

Improving the accuracy of the tidal model attribution is therefore arguably the most important aspect of the modelling process to be explored in future iterations of the product. Modelling a single location per epoch, similar to the method of Murray et al. (2012) is a practical method that fits well with the OTPS model and tile based architecture of the AGDC. However, there is no doubt that accuracy of the estimated tidal height degrades as the distance from the location or coastal complexity increases. This has the most obvious impact on attribution heights for DEM creation, but can also undermine the assumptions of the method when moving the analysis into the tidal domain.

Future work in the tidal attribution space will focus on adaptive methods to allow the local complexity and spatial variation of the OTPS outputs to define the scale of cells that are used to partition the data spatially. The aim being to minimise the variance of the OTPS derived heights within an optimised variable partition, replacing fixed cell sizes across all environments. This will enable complex coastal systems to be modelled at a smaller scale, driven by the tidal variation of the model itself. We would expect this to significantly improve the capacity to generate DEM data from the model, reduce modelling uncertainties, and help to isolate coastal instability detection features of the model. These improvements would likely enable DEM generation from shorter time-spans, by potentially reducing outliers in the ensembles of tidally sorted images; moving beyond the average DEM examples modelled over the 28 year time period in this work.

We openly recognise some of the practical limitations of the modelling process, data and product in some locations. For example, in micro

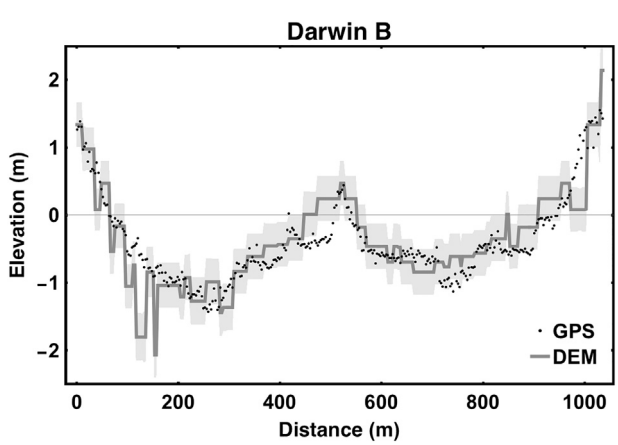

Fig. 19. DEM Validation for Darwin Harbour Transect B – DEM uncertainty range of ±1.96σ shown in grey.

Table 2
OTPS High & Low Tide Heights for Moreton Bay (153-028) and Darwin (130-013) – Observed (LOT and HOT for the AGDC time series archive), Interval Median (Median heights for the 0–10% and 80–100% Tidal Intervals) and Modelled (High and Low tide heights for a 12mth OTPS model run).

MSL(m)	Observed	Interval Median	Modelled
Moreton Bay			
High	1.25	1.01	1.31
Low	−0.68	−0.55	−0.95
Darwin			
High	2.84	2.10	3.39
Low	−2.88	−2.4	−3.5

tidal and/or steep sloping tidal regions where the spatial extent of the intertidal zone is small, the 25 m pixel resolution of the data limits the effectiveness and information that can be retrieved. Additionally, the model is restricted to mapping portions of the intertidal zone where water coverage is visible. Hence, areas of mangrove and vegetation cover, where underlying water is obscured from the satellite, are considered land by the algorithm.

6. Conclusions

In this paper we have introduced an automated continental scale method for modelling the intertidal extent and topography of Australia's coastline.

We have illustrated a conceptual model which leverages the full 28 year time series of Landsat data in the AGDC, and reframes the analysis based on continental scale tidal modelling. The relationship between the data and the new tidal domain enables ensemble analysis that deals with a number of generalizations and uncertainties in the process, as well as providing potential for examining further aspects of coastal instability.

To our knowledge this is first continental scale application that derives a relative elevation profile & topography of the intertidal zone. This extends the applications of the data set beyond area and extent mapping, enabling a new suite of use cases that require a more detailed understanding of the intertidal zone, such as hydrodynamic modelling. Implementing a compositing methodology has allowed us to overcome many of the data quality and noise issues encountered with single or limited scene applications. As the composite approach draws from all the available data, the model can be continually improved as future data is acquired, calibrated and ingested into the AGDC platform.

In future work the focus will be on improving the spatial accuracy of the tidal modelling process, to underpin improved digital elevation modelling from the product. This would enable provision of cost effective continental scale elevation data; complementing existing holdings and improving integration of terrestrial and bathymetric elevation data sets in the coastal zone.

Data availability

The Intertidal Extents Model (ITEM) products and data developed in this research can be downloaded from Geoscience Australia's online catalogue at http://www.ga.gov.au/metadata-gateway/metadata/record/100600, and viewed online via webserver at http://www.ga.gov.au/interactive-maps/#/theme/earthobservation/map/intertidal.

The location data for the tidal post modelling is available via request from the corresponding author.

Acknowledgments

The authors would like to thank Jin Li, Norman Mueller and three anonymous reviewers for valuable comments and suggestions. We would also like to thank individuals and organisations that provided validation data for our study. The RTK GPS data used in Moreton Bay, QLD was provided by Tim Danaher, NSW Office of Environment and Heritage. The RTK GPS data used in Darwin Harbour, NT was provided by HydroSurvey Australia, with the permission of GHD and Power & Water Corporation, NT.

This research was undertaken with the assistance of resources from the National Computational Infrastructure (NCI), which is supported by the Australian Government.

This paper is published with the permission of the Chief Executive Officer, Geoscience Australia.

Appendix A

The aim of our framework is to perform a regression of the form

$$y_i = f(t_i) + \epsilon_i$$

where y_i is a p-dimensional vector of NDWI pixels (recall that $p = 4000 \times 4000 = 16 \times 10^6$ in our case) for each observation $i \in \{1, 2, \ldots, n\}$, the t_i are the observation times, and ϵ_i is a p-dimensional vector of independent and identically distributed sub-Gaussian noise variables with mean $\mathbb{E}[\epsilon_i] = 0$ and variance $s^2 = \mathbb{E}[\epsilon_i^2]$ for all i. The crux of our approach is, due to lack of fine temporal sampling of observations, to perform a 'change of time' from true observation acquisition time to (approximate) tidal height through the use of an ancillary physics model for tides (Laplace's tidal equations). We define the tidal height $h(t)$ for some representative pixel and since we are learning the model f in a batch setting (i.e., all our observations are available), we determine the heights for all observation times t_i and are able to calculate the global maximum $h_{max} = \max\{h(t_1), h(t_2), \ldots, h(t_n)\}$ and global minimum $h_{min} = \min\{h(t_1), h(t_2), \ldots, h(t_n)\}$. This allows us to map observations onto the unit circle through the mapping.

$$h\sim(t) = 2\pi \frac{h_{max} - h(t)}{h_{max} - h_{min}}.$$

Performing a 'change of time' in our model, we obtain

$$y\sim_i = f(h\sim(t_i)) + \epsilon_i$$

which is a regression for NDWI value given tidal height. Since we believe that at some pixels there will be a sharp change from dry to wet as the tide rises, we propose that f should be a k-piecewise linear of the form

$$f(x) = \begin{cases} f_1(x), & \alpha_0 \le x < \alpha_1 \\ f_2(x), & \alpha_1 \le x < \alpha_2 \\ & \vdots \\ f_k(x), & \alpha_{k-1} \le x < \alpha_k \end{cases}$$

where the breaks $\alpha_0, \alpha_1, \ldots, \alpha_k$ are to be determined. Typically, a 'segmented regression' of this form can be difficult to solve as the breaks need to be determined from the data. We have taken the approach to determine these break points using a uniform partition our observed tidal height range, that is, we ensure the breaks are chosen so that $\alpha_0 = 0, \alpha_1 = 2\pi/10, \ldots, \alpha_k = 2\pi$ so that we have 10 intervals. Since we use one height $h_i = h\sim(t_i)$ for each p-dimensional vector y_i and due to observational errors, the heights in each bucket $[\alpha_i, \alpha_{i+1})$ can be quite noisy. As such, instead of using a standard least-squares regression to estimate the functions $f_1, f_2, \ldots, f_k$, we use a form of quantile regression called least absolute deviation or L^1-norm regression given by

$$f_i(x) = \mathrm{argmin}_x \sum_{j=1}^{m_i} |x - y_{(j)}|$$

where the $y_{(1)}, \ldots, y_{(m_i)}$ are the m_i p-dimensional vectors of NDWI pixels associated with the i'th percentile bucket of tidal heights. The argmin should be understood in a coordinate-wise sense with respect to the p-dimensional vectors. The solution of this regression is given by the (coordinate-wise) median of the $y_{(1)}, \ldots, y_{(m_i)}$ vectors. In other words, $f_i(x) = \mathrm{median}(y_{(1)}, \ldots, y_{(m_i)})$. This gives us our model for the p-dimensional vector of NDWI pixels $y\sim$ for a given tidal height (or alternatively, median NDWI image). To obtain a model of tidal extent we classified each pixel as water or not-water using a simple threshold on the median NDWI image. We expect that since the population distribution for NDWI has support $[-1.1]$ as it is a band ratio, the median m should be close to zero is it is a distribution that encompasses NDWI values from across the whole continent. Applying classic statistical theory and neglecting the bounded support of the NDWI distribution, the sampling distribution of the median is asymptotically normal with mean m and variance $1/[4\, n\, \phi(m)]$ where ϕ is the population distribution of NDWI and n is the sample size. For a simple unsupervised classification, a simple threshold is applied to the NDWI image to classify water.

References

Airoldi, L., Beck, M.W., 2007. Loss, status and trends for coastal marine habitats of Europe. Oceanogr. Mar. Biol. Annu. Rev. 345–405.

Barndorff-Nielsen, O.E., Shiryaev, A., 2010. Change of Time and Change of Measure, Advanced Series on Statistical Science and Applied Probability. World Scientific.

Bell, P.S., Bird, C.O., Plater, A.J., 2016. A temporal waterline approach to mapping intertidal areas using X-band marine radar. Coast. Eng. 107:84–101. http://dx.doi.org/10.1016/j.coastaleng.2015.09.009.

Brockmann, C., Stelzer, K., 2008. Optical remote sensing of intertidal flats. In: Barale, V., Gade, M. (Eds.), Remote Sensing of the European Seas. Springer, Netherlands, pp. 117–128.

Chen, Y., Dong, J., Xiao, X., Zhang, M., Tian, B., Zhou, Y., Li, B., Ma, Z., 2016. Land claim and loss of tidal flats in the Yangtze estuary. Sci. Rep. 6:24018. http://dx.doi.org/10.1038/srep24018.

Chen, L.C., Rau, J.Y., 1998. Detection of shoreline changes for tideland areas using multi-temporal satellite images. Int. J. Remote Sens. 19, 3383–3397.

Clemens, R.S., Rogers, D.I., Hansen, B.D., Gosbell, K., Minton, C.D.T., Straw, P., Bamford, M., Woehler, E.J., Milton, D.A., Weston, M.A., Venables, B., Weller, D., Hassell, C., Rutherford, B., Onton, K., Herrod, A., Studds, C.E., Choi, C.-Y., Dhanjal-Adams, K.L., Murray, N.J., Skilleter, G.A., Fuller, R.A., 2016. Continental-scale decreases in shorebird populations in Australia. Emu 116:119. http://dx.doi.org/10.1071/MU15056.

Cracknell, A.P., 1999. Remote sensing techniques in estuaries and coastal zones an update. Int. J. Remote Sens. 20:485–496. http://dx.doi.org/10.1080/014311699213280.

Danaher, T., Collet, L., 2006. Development, Optimisation and Multi-Temporal Application of a Simple Landsat Based Water Index. In: Proceedings of the 13th Australasian Remote Sensing and Photogrammetry Conference. Presented at the 13th Australasian Remote Sensing and Photogrammetry Conference, 20-24 November 2006, Canberra, ACT.

Dhanjal-Adams, K.L., Hanson, J.O., Murray, N.J., Phinn, S.R., Wingate, V.R., Mustin, K., Lee, J.R., Allan, J.R., Cappadonna, J.L., Studds, C.E., Clemens, R.S., Roelfsema, C.M., Fuller, R.A., 2016. The distribution and protection of intertidal habitats in Australia. Emu 116:208. http://dx.doi.org/10.1071/MU15046.

Donchyts, G., Schellekens, J., Winsemius, H., Eisemann, E., van de Giesen, N., 2016. A 30 m resolution surface water mask including estimation of positional and thematic differences using Landsat 8, SRTM and OpenStreetMap: a case study in the Murray-Darling Basin, Australia. Remote Sens. 8:386. http://dx.doi.org/10.3390/rs8050386.

Egbert, G.D., Erofeeva, S.Y., 2002. Efficient inverse modeling of Barotropic Ocean tides. J. Atmos. Ocean. Technol. 19:183–204. http://dx.doi.org/10.1175/1520-0426(2002)019<0183:EIMOBO>2.0.CO;2.

Egbert, G.D., Erofeeva, S.Y., 2010. The OSU TOPEX/Poseiden Global Inverse Solution TPXO [WWW Document]. TPXO8-Atlas Version 10. (URL http://volkov.oce.orst.edu/tides/global.html (accessed 2.15.16)).

Feyisa, G.L., Meilby, H., Fensholt, R., Proud, S.R., 2014. Automated water extraction index: a new technique for surface water mapping using Landsat imagery. Remote Sens. Environ. 140:23–35. http://dx.doi.org/10.1016/j.rse.2013.08.029.

Fisher, A., Flood, N., Danaher, T., 2016. Comparing Landsat water index methods for automated water classification in eastern Australia. Remote Sens. Environ. 175:167–182. http://dx.doi.org/10.1016/j.rse.2015.12.055.

Flood, N., 2013. Seasonal composite Landsat TM/ETM+ images using the Medoid (a multi-dimensional median). Remote Sens. 5:6481–6500. http://dx.doi.org/10.3390/rs5126481.

Galbraith, H., Jones, R., Park, R., Clough, J., Herrod-Julius, S., Harrington, B., Page, G., 2002. Global climate change and sea level rise: potential losses of intertidal habitat for shorebirds. Waterbirds Int. J. Waterbird Biol. 25, 173–183.

Geoscience Australia, 2015. Australian Reflectance Grid (ARG25) Product Description v1.1. http://dx.doi.org/10.4225/25/5487CC0D4F40B.

Griffiths, P., van der Linden, S., Kuemmerle, T., Hostert, P., 2013. A pixel-based Landsat compositing algorithm for large area land cover mapping. IEEE J. Sel. Top. Appl. Earth Obs. Remote Sens. 6:2088–2101. http://dx.doi.org/10.1109/JSTARS.2012.2228167.

Healy, T.R., Wang, Y., Healy, J.-A. (Eds.), 2002. Muddy Coasts of the World: Processes, Deposits, and Function. Gulf Professional Publishing.

Hovmöller, E., 1949. The trough-and-ridge diagram. Tellus 1:62–66. http://dx.doi.org/10.1111/j.2153-3490.1949.tb01260.x.

HydroSurvey Australia, 2009. Report for Bathymetric and Benthic Survey of the Proposed East Point Outfall (Part Two - Bathymetric Report No. Survey No. 018_08). Power and Water Corporation/GHD.

Kirwan, M.L., Megonigal, J.P., 2013. Tidal wetland stability in the face of human impacts and sea-level rise. Nature 504:53–60. http://dx.doi.org/10.1038/nature12856.

Kordi, M.N., Collins, L.B., O'Leary, M., Stevens, A., 2016. ReefKIM: an integrated geodatabase for sustainable management of the Kimberley Reefs, North West Australia. Ocean Coast. Manag. 119:234–243. http://dx.doi.org/10.1016/j.ocecoaman.2015.11.004.

Lewis, A., Lymburner, L., Purss, M.B.J., Brooke, B., Evans, B., Ip, A., Dekker, A.G., Irons, J.R., Minchin, S., Mueller, N., Oliver, S., Roberts, D., Ryan, B., Thankappan, M., Woodcock, R., Wyborn, L., 2015. Rapid, high-resolution detection of environmental change over continental scales from satellite data – the earth observation data cube. Int. J. Digital Earth 0:1–6. http://dx.doi.org/10.1080/17538947.2015.1111952.

Li, W., Gong, P., 2016. Continuous monitoring of coastline dynamics in western Florida with a 30-year time series of Landsat imagery. Remote Sens. Environ. 179:196–209. http://dx.doi.org/10.1016/j.rse.2016.03.031.

Li, F., Jupp, D.L.B., Thankappan, M., Lymburner, L., Mueller, N., Lewis, A., Held, A., 2012. A physics-based atmospheric and BRDF correction for Landsat data over mountainous terrain. Remote Sens. Environ. 124:756–770. http://dx.doi.org/10.1016/j.rse.2012.06.018.

Liu, Y., Li, M., Zhou, M., Yang, K., Mao, L., 2013. Quantitative analysis of the waterline method for topographical mapping of tidal flats: a case study in the Dongsha sandbank, China. Remote Sens. 5:6138–6158. http://dx.doi.org/10.3390/rs5116138.

Liu, Y., Song, P., Peng, J., Ye, C., 2012. A physical explanation of the variation in threshold for delineating terrestrial water surfaces from multi-temporal images: effects of radiometric correction. Int. J. Remote Sens. 33:5862–5875. http://dx.doi.org/10.1080/01431161.2012.675452.

Loveland, T.R., Dwyer, J.L., 2012. Landsat: building a strong future. Remote Sens. Environ. 122:22–29. http://dx.doi.org/10.1016/j.rse.2011.09.022.

Mason, D.C., Amin, M., Davenport, I.J., Flather, R.A., Robinson, G.J., Smith, J.A., 1999. Measurement of recent intertidal sediment transport in morecambe bay using the waterline method. Estuar. Coast. Shelf Sci. 49:427–456. http://dx.doi.org/10.1006/ecss.1999.0508.

Mason, D.C., Davenport, I.J., Robinson, G.J., Flather, R.A., McCartney, B.S., 1995. Construction of an inter-tidal digital elevation model by the "Water-Line" method. Geophys. Res. Lett. 22:3187–3190. http://dx.doi.org/10.1029/95GL03168.

Mason, D.C., Hill, D., Davenport, I., Flather, R., Robinson, G., 1997. Improving inter-tidal digital elevation models constructed by the waterline technique. Presented at the Third ERS Symposium on Space at the service of our Environment, p. 1079.

Mason, D.C., Scott, T.R., Dance, S.L., 2010. Remote sensing of intertidal morphological change in Morecambe Bay, U.K., between 1991 and 2007. Estuar. Coast. Shelf Sci. 87:487–496. http://dx.doi.org/10.1016/j.ecss.2010.01.015.

McFeeters, S.K., 1996. The use of the Normalized Difference Water Index (NDWI) in the delineation of open water features. Int. J. Remote Sens. 17:1425–1432. http://dx.doi.org/10.1080/01431169608948714.

Murray, N.J., Clemens, R.S., Phinn, S.R., Possingham, H.P., Fuller, R.A., 2014. Tracking the rapid loss of tidal wetlands in the Yellow Sea. Front. Ecol. Environ. 12:267–272. http://dx.doi.org/10.1890/130260.

Murray, N.J., Phinn, S.R., Clemens, R.S., Roelfsema, C.M., Fuller, R.A., 2012. Continental scale mapping of tidal flats across East Asia using the Landsat archive. Remote Sens. 4:3417–3426. http://dx.doi.org/10.3390/rs4113417.

Park, W., Lee, Y.-K., Shin, J.-S., Won, J.-S., 2013. A tidal correction model for near-infrared (NIR) reflectance over tidal flats. Remote Sens. Lett. 4:833–842. http://dx.doi.org/10.1080/2150704X.2013.791955.

Rokni, K., Ahmad, A., Selamat, A., Hazini, S., 2014. Water feature extraction and change detection using Multitemporal Landsat imagery. Remote Sens. 6:4173–4189. http://dx.doi.org/10.3390/rs6054173.

Roy, D.P., Ju, J., Kline, K., Scaramuzza, P.L., Kovalskyy, V., Hansen, M., Loveland, T.R., Vermote, E., Zhang, C., 2010. Web-enabled Landsat Data (WELD): Landsat ETM+ composited mosaics of the conterminous United States. Remote Sens. Environ. 114:35–49. http://dx.doi.org/10.1016/j.rse.2009.08.011.

Ryu, J.-H., Kim, C.-H., Lee, Y.-K., Won, J.-S., Chun, S.-S., Lee, S., 2008. Detecting the intertidal morphologic change using satellite data. Estuar. Coast. Shelf Sci. 78:623–632. http://dx.doi.org/10.1016/j.ecss.2008.01.020.

Ryu, J.-H., Won, J.-S., Min, K.D., 2002. Waterline extraction from Landsat TM data in a tidal flat: a case study in Gomso Bay, Korea. Remote Sens. Environ. 83:442–456. http://dx.doi.org/10.1016/S0034-4257(02)00059-7.

Sixsmith, J., Oliver, S., Lymburner, L., 2013. A hybrid approach to automated Landsat pixel quality. Geoscience and Remote Sensing Symposium (IGARSS), 2013 IEEE International. Presented at the Geoscience and Remote Sensing Symposium (IGARSS), 2013 IEEE International:pp. 4146–4149 http://dx.doi.org/10.1109/IGARSS.2013.6723746.

White, J.C., Wulder, M.A., Hobart, G.W., Luther, J.E., Hermosilla, T., Griffiths, P., Coops, N.C., Hall, R.J., Hostert, P., Dyk, A., Guindon, L., 2014. Pixel-based image compositing for large-area dense time series applications and science. Can. J. Remote. Sens. 40:192–212. http://dx.doi.org/10.1080/07038992.2014.945827.

Xu, H., 2006. Modification of normalised difference water index (NDWI) to enhance open water features in remotely sensed imagery. Int. J. Remote Sens. 27:3025–3033. http://dx.doi.org/10.1080/01431160600589179.

Zhao, B., Guo, H., Yan, Y., Wang, Q., Li, B., 2008. A simple waterline approach for tidelands using multi-temporal satellite images: a case study in the Yangtze Delta. Estuar. Coast. Shelf Sci. 77:134–142. http://dx.doi.org/10.1016/j.ecss.2007.09.022.

Zhu, Z., Woodcock, C.E., 2012. Object-based cloud and cloud shadow detection in Landsat imagery. Remote Sens. Environ. 118:83–94. http://dx.doi.org/10.1016/j.rse.2011.10.028.

View publication stats